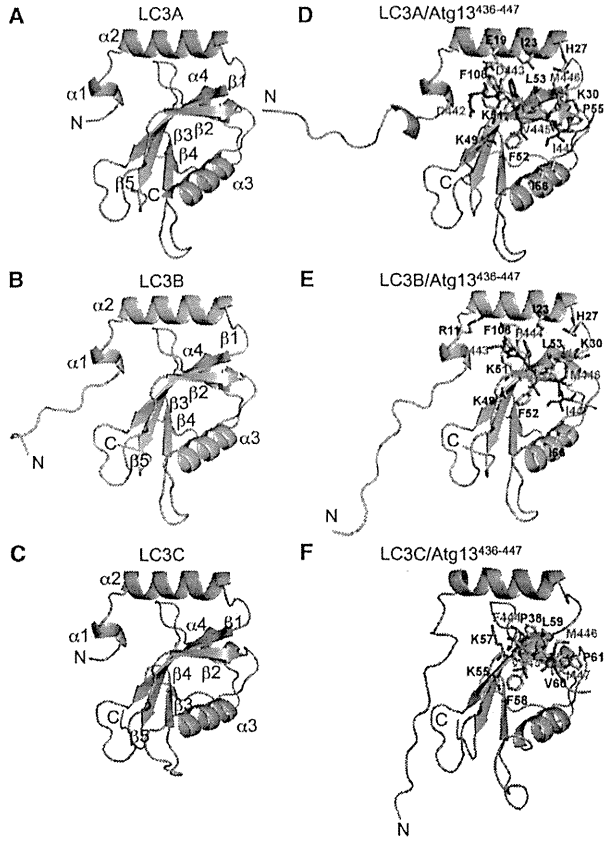

Figure 4. Overall Structures of Uncomplexed Form and Atg13 LIR-Fused LC3 Isoforms

Structures of uncomplexed form (A–C) and Atg13 LIR-fused LC3 isoforms (D–F) are represented by ribbon diagrams and colored in green (LC3A), cyan (LC3B), and orange (LC3C). LIR in symmetry-related molecules (magenta) and its interaction residues are shown in stick representation. Oxygen, nitrogen, and sulfur atoms are shown in red, blue, and yellow, respectively. The secondary structure was defined by the DSSP program (Kabsch and Sander, 1983).

E19D to investigate the LC3B binding. LC3B has significantly poorer binding to the Atg13 LIR compared with LC3A and LC3C (LC3A, 18.3 ± 0.6 μM; LC3B, 52 ± 7 μM; LC3C, 13 ± 6 μM), and Glu19 is the only binding residue that is conserved between LC3A and LC3C, but not LC3B (LC3A and LC3C, Glu; LC3B, Asp). Therefore, we predicted that a mutation at this site would have a significant effect on binding. The K49A and K49F mutations were designed to mimic the open and closed surface of LC3A, whereas the K51A, F52A, and L53A mutations were designed to probe the bottom floor of the binding site (Figure 5). $LC3A^{E19D}$ showed a slight increase in its binding ability to the Atg13 LIR (112 ± 2%). Interestingly, K49A mutation resulted in a marked increase 182 ± 2%, which presumably reflects the "always open" binding pocket formed by the methyl group of K49A. On the other hand, K51A and L53A mutations demonstrated reduced binding abilities (K51A, 29 ± 2%; L53A, 41 ± 1%, Figure 6D). Unfortunately, $LC3A^{K49F}$ and $LC3A^{F52A}$ aggregated on the sensor chip, increasing the resonance signals not only in Atg13 LIR immobilized flow cells but also in reference flow cells (data not shown), and the accurate binding abilities could not be estimated. The dissociation constants of K49A and K51A as the highest and the lowest binding ability mutants are measured by an SPR biosensor (Figure S5). The KD values for $LC3A^{K49A}$ and $LC3A^{K51A}$ to GST-$Atg13^{411-447}$ were 6.6 ± 1.0 μM and 150 ± 2.6 μM, respectively. To verify the Atg13/LC3 interaction in vivo, we performed pulldown assay using HEK293 cells that expressed OSF-LC3A (WT, K49A, and K51A) and Myc-tagged ULK1 complex (Myc-ULK1, Myc-Atg101, Myc-FIP200, and Myc-Atg13) under nutrient-rich and starvation conditions (Figure S6). K49A mutant showed higher binding ability to the ULK1 complex than did WT; on the other hand, K51A mutation was similar or slightly decreased the binding ability to the ULK1 complex.

Movement of Lys49 Is Conserved in Mammalian LC3 Homologs

To investigate whether the side-chain configuration of Lys49 is conserved in LC3 homologs, we compared our LC3 structures with the eight reported LC3 homologs (Figure 7). The PDB contains four uncomplexed structures (ratLC3, 1UGM, Sugawara et al., 2004; GABARAP, 1KJT, Bavro et al., 2002; GATE-16, 1EO6, Paz et al., 2000; and Atg8, 2KWC, Kumeta et al., 2010) and four types of LIR-bound structures (LC3B/p62, 2ZJD, Ichimura et al., 2008; and 2K6Q, Noda et al., 2008; GABARAP/synthetic peptide, 3D32, Weiergräber et al., 2008; GABARAPL-1/NBR1, 2L8J, Rozenknop et al., 2011; and Atg8/Atg19, 2ZPN, Noda et al., 2008).

In the uncomplexed structures, except for Atg8, a yeast LC3 homolog, the side-chain carbon atoms of the equivalent Lys49 are located within 4 Å from the aromatic portion of Phe or Tyr at strand β2 (Lys49 and Phe52 in rat LC3 and Lys46 and Tyr49 in GATE-16, GABARAP, and Atg8 correspond to Lys49 and Phe52 in human LC3A). Thus, it seems that the residues corresponding to Lys49 of LC3A in the mammalian homologs cover the hydrophobic surfaces by interacting with these aromatic residues. In contrast, the side-chain of Lys46 in Atg8 faces away from Tyr49 and does not cover the interaction surface.

In the complexed structure of LC3B/p62, Lys49 does not interact with p62 LIR, although it undergoes a large structural rearrangement. In the GABARAP/synthetic peptide structure, the peptide forms an α-helix, instead of a parallel β sheet with strand β2 of GABARAP like other complex structures, and Lys46 moves only slightly upon peptide binding to break the hydrophobic interaction with Tyr49. Lys46 in the GABARAPL-1/NBR1 complex structure is oriented in the opposite direction to NBR1 LIR. The uncomplexed structure of GABARAPL-1 has not been reported; however, as mentioned above, the LIR interaction surface of GABARAP, which shares 87% identity with that of GABARAPL-1, is covered with a side-chain of Lys46. Taken together, these structural comparisons suggest that the movement of Lys49 side-chain is conserved in the mammalian LC3 proteins.

Lys49 Residue Plays Important Roles in Autophagosome Formation

To verify the importance of the interaction between Atg13 and the LC3 proteins in autophagosome formation, we established

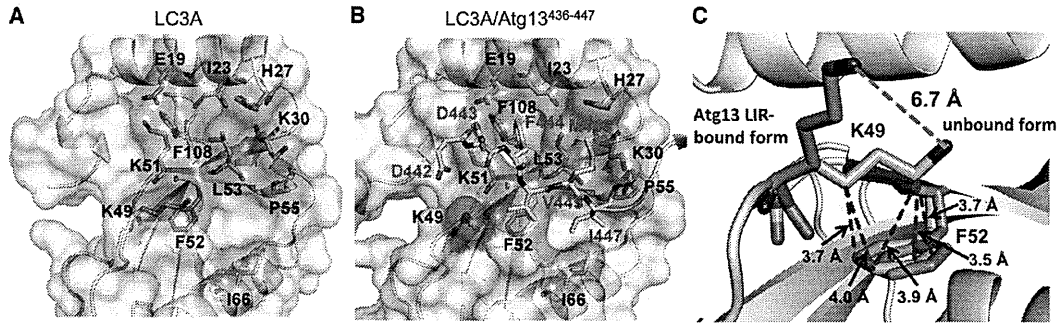

Figure 5. Structural Comparison between the Uncomplexed and the Atg13 LIR Complexed Forms of LC3A

(A and B) LC3A and LC3A/Atg13$^{436-447}$ are shown in ribbon and transparent surface representation. LIR and its interaction residues are shown in stick representation. Carbon atoms of LIR, Lys49, and other residues are colored yellow, magenta, and green, respectively. Oxygen and nitrogen atoms are in red and blue, respectively.

(C) Close-up view of Lys49 and Phe52. Carbon atoms of the uncomplexed form and Atg13 LIR complexed form of LC3A are colored in orange and cyan, respectively.

mouse embryonic fibroblast cells stably expressing GFP-tagged LC3A^{WT}, LC3A^{K49A}, or LC3A^{K51A} and tested for LC3A positive puncta formation (Figures 8A and 8B). Western blotting showed similar GFP-LC3A expression levels in each stable cell line (Figure S7). LC3A^{WT} formed puncta in the cells with nutrient-rich conditions (39 ± 12 dots/cell), and the number of puncta was significantly increased under starvation conditions (134 ± 18 dots/cell). The number of puncta further increased (188 ± 29 dots/cell) after treatment with Baf A1, an inhibitor of lysosomal acidification. Taken together, these data indicate that GFP-LC3A^{WT}-positive autophagosomes are under active autophagy flux.

Surprisingly, cell lines expressing GFP-tagged LC3A^{K49A} and LC3A^{K51A} did not form any puncta in nutrient-rich conditions (2 ± 1 dots/cell in K49A; 12 ± 7 dots/cell in K51A) and formed even fewer puncta in starvation conditions (88 ± 36 dots/cell in K49A; 100 ± 15 dots/cell in K51A), despite the observation above that LC3A^{K49A} has significantly increased binding to the Atg13 LIR, whereas LC3A^{K51A} has reduced the binding abilities (Figure 6D). Moreover, LC3-positive puncta for LC3A^{K49A} and LC3A^{K51A} were also fewer than those of LC3A^{WT} in the presence of Baf A1, indicating that autophagy flux was decreased. These data also suggest that the reduced number of puncta formation results from the defect in autophagosome formation, but not enhancement of autophagosome degradation. Overall, these data suggest that there is a specific range, at least from 10 μM (LC3C) to 60 μM (LC3B), with respect to Atg13 LIR binding affinity for LC3A. If either too high or too low, autophagosome formation is decreased.

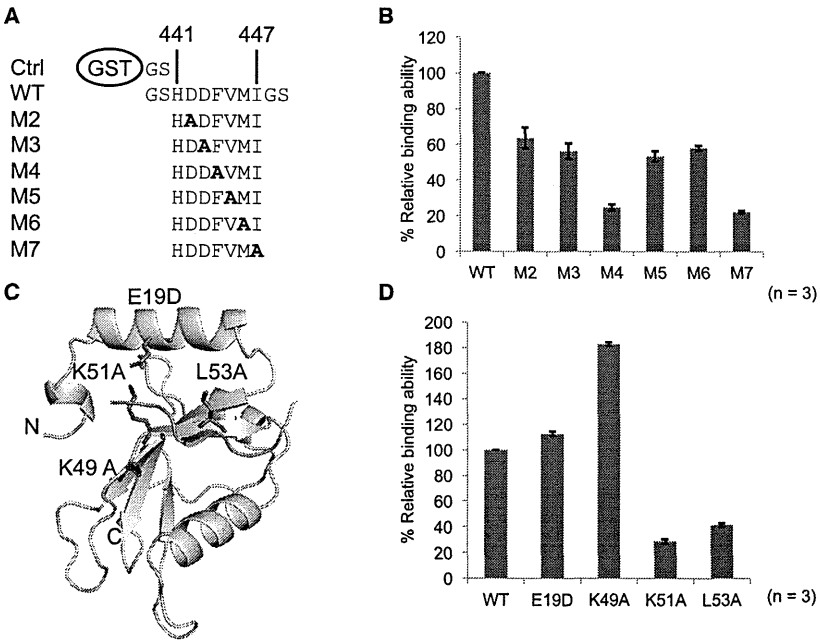

Figure 6. Mutational Analyses of the Interactions between Atg13 and LC3

(A) Schematic representation of mutants for Ala scanning.

(B and D) Relative binding abilities of point mutants of Atg13 or LC3A compared with WT were measured by an SPR biosensor and expressed in percentages. Each value represents the mean ± SD. The sensorgrams are shown in Figure S4.

(C) Ribbon diagram of the Atg13 LIR-fused LC3A structure highlighting the substituted residues (red stick representation) and the LIR (ribbon representation and colored line).

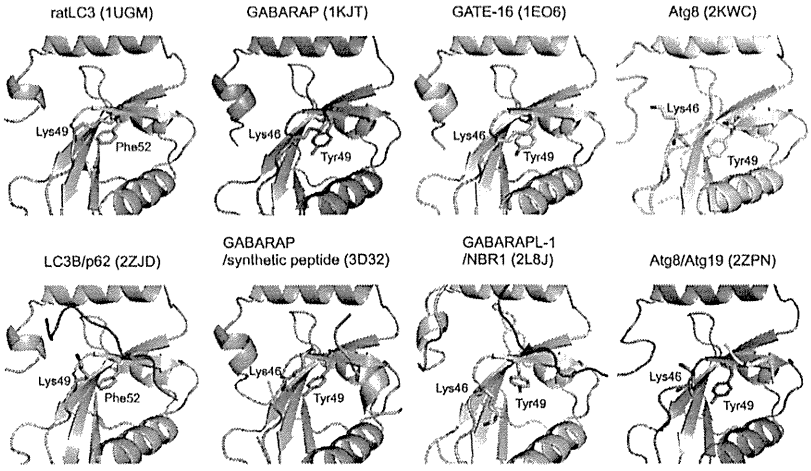

Figure 7. Structural Comparison of Lys49 Side-Chain Configuration among LC3 Family Proteins

Corresponding residues to Lys49 and Phe52 of LC3A in ratLC3 (PDB code 1UGM), GABARAP (1JKT), GATE-16 (1EO6), and Atg8 (2KWC) as uncomplexed form, and LC3B/p62 (2ZJD), GABARAP/synthetic peptide (3D32), GABARAP-L1/NBR1 (2L8J), and Atg8/Atg19 (2ZPN) as LIR-bound form are shown in ribbon representation in green, magenta, cyan, magenta, yellow, salmon, orange, lime green, and slate, and the peptides are colored marine blue, lime green, purple, and yellow orange, respectively. Side-chain atoms are colored red for oxygen and blue for nitrogen.

DISCUSSION

Recently Alemu et al. (2012) reported that Atg8 family proteins interact with ULK1/2, FIP200, and Atg13 and that this interaction is mediated by a LIR motif, which together suggested that Atg8 proteins play a role in scaffolding for the Atg1/ULK1 complex assembly. However, the molecular mechanism underpinning the interaction between the LIR and Atg8 family proteins was unclear. In this study, we have determined the crystal structures of the three LC3 isoforms in complex with the Atg13 LIR to delineate the key interactions between the two proteins, and we verified them by mutational analysis and in vivo studies.

We have identified that the LC3 binding site of Atg13 spans residues 441–447 (HDDFVMI) and provides the structural basis for the binding. Although the LIR motif was originally defined as xxxW/YxxL/I/V, it was recently reported that a Phe residue can also be tolerated at the aromatic position (Satoo et al., 2009; Kraft et al., 2012; Alemu et al., 2012). Our structural studies of the LC3 isoforms demonstrate that the W-site is deep enough to bury the bulky aromatic side-chains (Figure 5). A comparison of the Atg13 LIR and p62 LIR in those complexed structures shows that the LC3 residues that interact with the Atg13 aromatic residue (Atg13 LIR, Phe; p62 LIR, Trp) are located at the bottom of the hydrophobic pocket (Table S1). According to Alemu et al. (2012), Trp is the most abundant amino acid at the aromatic position in the LIR motifs (Trp, 14; Phe, 8; Tyr, 4; in 26 LIR motifs), suggesting that Trp forms more stable hydrophobic interactions with the W-site than Phe and Trp. However the W-site is not formed without the LIR binding, in contrast with the L-site, which is open even in the uncomplexed form. Our SPR biosensor analysis (Figure 6), along with previous reports (Noda et al., 2008; Alemu et al., 2012), demonstrates that mutation of the Leu/Ile/Val position significantly reduces binding. Taken together, these suggest that the L-site recognizes Leu/Ile/Val in the LIR first, and then a structural rearrangement occurs to open the W-site. However, binding to the L-site is not sufficient to stabilize the interaction alone, given that mutation of the aromatic residue in the LIR also significantly decreases the binding affinity of the Atg13 peptide to LC3. Accordingly, the W-site probably locks the interaction by burying the bulky part of an aromatic residue.

Our structural analysis demonstrates that Lys49 undergoes a significant structural rearrangement upon the LIR binding (Figure 5). In the uncomplexed structures, the side-chain of Lys49 makes hydrophobic interactions with the aromatic ring of Phe52, closing over the W-site and preventing binding. However, in our complexed structures, Val445 in the Atg13 LIR exists on the surface of Phe52, and Lys49 rearranges its conformation to interact with Val445, which is not observed in the complex structure with p62 LIR. Moreover, our SPR biosensor experiments demonstrate that the LC3A^{K49A} mutant, which we predicted would be in an open conformation, increased the relative binding ability to Atg13 LIR (Figure 6D). These data suggested that the interaction between Lys49 and Val445 does not stabilize this complex, but that the side-chain conformational change of Lys49 is important for recognition of the LIR, probably to open the surface covered by Lys49 and expose the W-site. The structural comparison revealed that this Lys49 side-chain movement is conserved in GABARAPs as well as LC3s, but not in yeast Atg8. Thus, it seems that this Lys49 gating mechanism may play a role in the LIR recognition for the LC3 family proteins, evolving after the last common ancestor.

Taken together, the LIR recognition mechanism of mammalian LC3 family proteins is explained as shown in Figure 9.

(1) The side-chain of Lys49 restricts access of LIR motif to the binding surface (Figure 9C, magenta),
(2) in response to the LIR motif approaching, the L-site is changed slightly and accepts branched-chain amino acids (Leu/Ile/Val; Figure 9B),
(3) the amino acid next to an aromatic residue in LIR dislocates the side-chain of Lys49 from the binding surface consisting of Phe52 (Figure 9C, green),
(4) the W-site then becomes available to accommodate the aromatic residue of Atg13, and
(5) by flipping the side-chains of Ile23 and Leu53, an aromatic residue is locked (Figure 9D).

Thus, not only are the W- and L-sites required for binding, but Lys49 is the key residue for LIR recognition, in particular controlling the LIR access to the interaction surface.

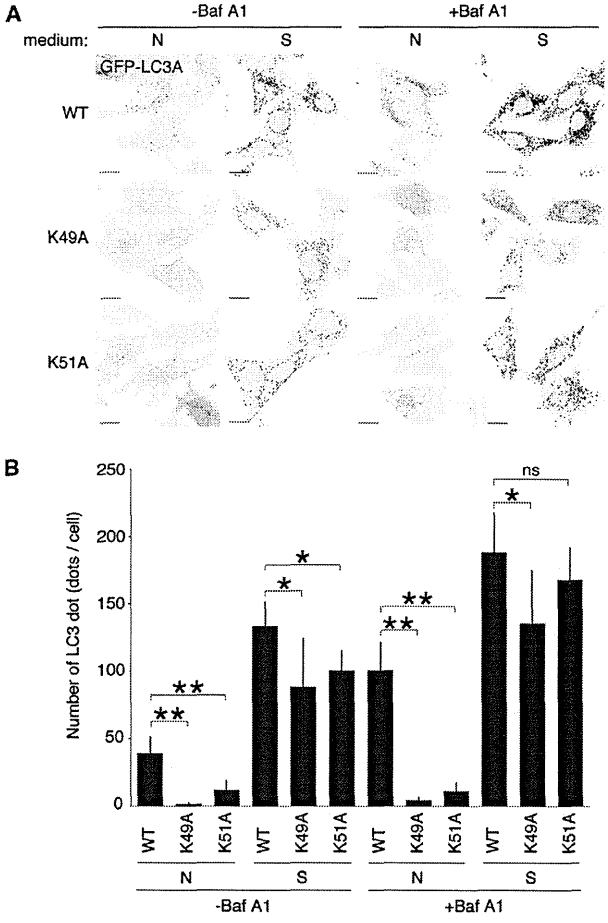

Figure 8. The Effect of LC3 Mutations on Autophagosome Formation and Autophagy Flux

(A) MEFs stably expressing the indicated constructs were cultured in nutrient-rich medium (N) or EBSS (S) with or without bafilomycin A1 (Baf A1) for 1 hr. Bars indicate 20 μm.

(B) The numbers of LC3 puncta in cells were counted in >30 cells. Each value represents the mean ± SD. Statistical analysis was performed by Student's t test: *$p < 0.05$, **$p < 0.01$; ns, not significant.

To establish the biological importance of Lys49, we assessed the effect of substituting LC3A Lys49 or Lys51 with Ala on autophagosome formation using fluorescence microscopy. Because the binding of $LC3A^{K49A}$ to the Atg13 LIR increased markedly as compared with $LC3A^{WT}$, we expected that this mutation would increase the number of autophagosomes under starvation conditions by enhancing the interaction with LIR. Surprisingly, however, both the K49A and K51A mutants showed a significant decrease in autophagosome formation, especially under nutrient-rich conditions, in which selective autophagy is predominant over macroautophagy induced by stimulus. On the other hand, under starvation conditions, where the Atg1/ULK1 complex is activated by TORC1 and initiates macroautophagy, the K49A mutation demonstrated a greater decrease in autophagosome formation than did K51A mutation, with or without Baf A1. Although this experiment cannot distinguish between specific binding partners, it demonstrates the importance of the Lys49 side-chain configuration in vivo and suggests that only a specific affinity between LC3 and its binding partners is required for recruiting substrates to the isolation membrane and proper autophagosome formation.

In conclusion, we proposed a LIR recognition mechanism for the mammalian LC3 family proteins, whereby LIR binding is regulated by Lys49 side-chain gating, and demonstrate that specific binding affinities (the expected range is from 10 μM to 60 μM) by this mechanism are required for recruiting its binding partners to autophagosome in both starvation-induced and selective autophagy.

EXPERIMENTAL PROCEDURES

Expression Plasmids

For the mammalian expression vectors, ULK1 complex subunits (Atg101, Atg13, ULK1, and FIP200), and LC3s, cDNA open reading frames (ORFs) were subcloned into KpnI/*Xho*I sites of pCAG-OSF or pCAG-Myc vectors, as described previously (Madaule et al., 1998; Bajorek et al., 2009). For yeast two-hybrid vectors, cDNA ORFs were subcloned into *Eco*RI/*Bam*HI sites (Atg13, Atg101, LC3A, and LC3C) or *Nco*I/*Bam*HI sites (GABARAP) of pGADT7 or pGBKT7. For retroviral expression vectors, LC3A cDNA ORFs were subcloned into *Eco*RV sites of pMRX retroviral vector. For bacterial expression vectors, Atg13 truncation mutants, $LC3A^{2-121}$, $LC3B^{2-119}$, and $LC3C^{8-125}$ were generated by PCR and inserted into pGEX-4T-1 (Atg13, *Bam*HI/*Eco*RI site; LC3A, *Eco*RI/*Sal*I site; LC3C, *Bam*HI/*Eco*RI site; GE Healthcare), pCold TF (Atg13, *Bam*HI/*Eco*RI site; Clontech), the *Bam*HI/*Eco*RI site of pET30 (Invitrogen) deleted S-tag, and Enterokinase site (designated pET30ΔSE) by QuickChange mutagenesis kit (Stratagene) using the oligonucleotide pair 5′-CTGGTGCCACGCGGATCCGAATTCGAGCTC-3′ and 5′-GAGCTCGAATT CGGATCCGCGTGGCACCAG-3′. For construction of the GST-fused peptide, the oligonucleotide pair (5′-GATCCTGAGATATCGACTCGAGG-3′ and 5′-AATTCCTCGAGTCGATATCTCAG-3′) was inserted into the *Bam*HI/*Eco*RI site of pGEX-4T-1, designated pGEX-4T_BS (*Bam*HI-Stop). The chimera proteins of Atg13 LIR-fused LC3 isoforms and GST-fused Atg13 LIR peptides were constructed by inserting a pair of double-stranded oligonucleotides into the *Bam*HI sites of pET30ΔSE/LC3 isoforms and pGEX-4T_BS, respectively. Point mutants of LC3A were generated using the QuickChange mutagenesis kit.

Cell Cultures

HEK293T and mouse embryonic fibroblast (MEF) cells were maintained in Dulbecco's modified Eagle's medium supplemented with 10% fetal calf serum. Stable transformants were selected in growth medium with 1 μg/ml puromycin. For immunofluorescence experiments, MEF cells were seeded onto coverslips and cotransfected at 50%–60% confluence.

Coprecipitation and Western Blotting Assays

HEK293T cells were seeded (3×10^6 cells/55 cm^2 dish) and cotransfected with each relevant expression plasmid (polyethylenimine 25,000 kDa; Polysciences), as described (Durocher et al., 2002). Cells were harvested 48 hr posttransfection by incubation in lysis buffer (50 mM Tris-HCl, pH 7.4, 150 mM NaCl) supplemented with protease inhibitor cocktail (Sigma) and 1% Triton X-100. Lysates were clarified by centrifugation (18,000 × *g*, 10 min, 4°C) and incubated with Strep-Tactin Sepharose for 2 hr (IBA). The resin was washed four times with wash buffer (20 mM Tris-HCl, pH 7.4, 150 mM NaCl) supplemented with 0.1% Triton X-100, and bound proteins were detected by mass spectrometry or western blotting.

Yeast Two-Hybrid Binding Assays

Directed yeast two-hybrid assays were performed using the Matchmaker GAL4 Yeast Two Hybrid 3 System (Clontech). Briefly, *Saccharomyces cerevisiae* AH-109 was cotransformed with pGADT7 or pGBKT7 cloning vector (Clontech) containing the inserts of interest. The transformed yeast colonies were grown for 3 days at 30°C on yeast-extract-peptone-dextrose plates

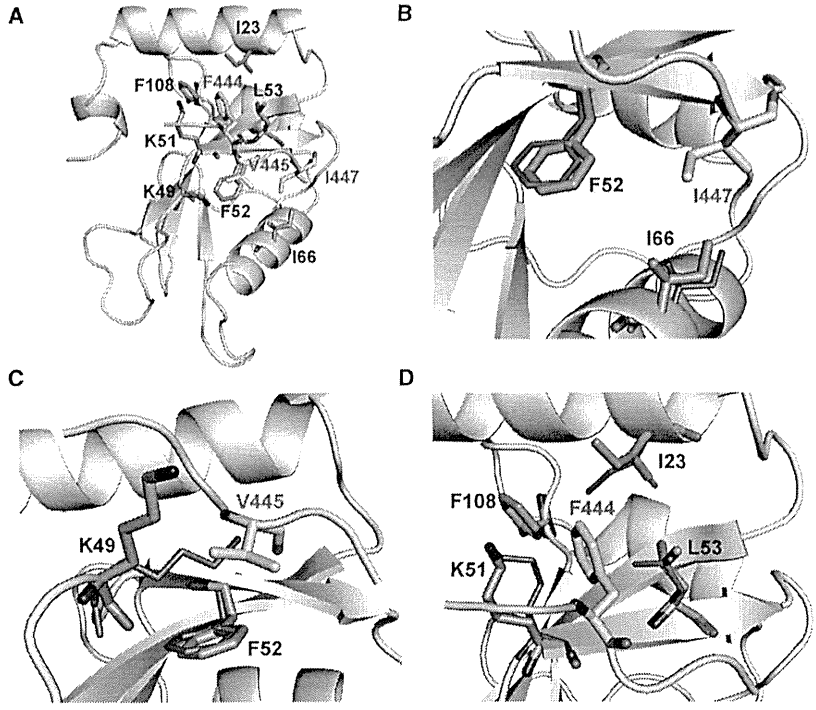

Figure 9. The Binding between LC3 and LIR Is Regulated by Structural Rearrangement of Lys49 Side-Chain and Hydrophobic Interaction by Phe444 and Ile447

(A) Ribbon diagram of LC3A and LIR colored white and yellow. Side chains of binding residues are shown in stick representation.

(B–D) Close-up views of the critical binding sites. The residues surrounding Phe444 (the W-site) (D) and Ile447 (the L-site) (B) undergo subtle structural rearrangement and form hydrophobic interactions. In the uncomplexed structure (C), the side-chain of Lys49 covers LIR interaction surface. Upon binding of LIR to LC3, the side-chain of Lys49 detached from Phe52 an open hydrophobic surface consisting of Lys49 and Phe52. Green and purple indicate the residues in the uncomplexed and LIR-bound structures, respectively.

with minus Leu, minus Trp selection. From 10 to 100 colonies were pooled, resuspended in a liquid culture of Sabourand dextrose broth (minus Leu, minus Trp), selected on Sabourand dextrose broth (minus Leu, minus Trp, minus Ade, minus His) plates, and allowed to grow for 3 days.

Purification of Recombinant Proteins and GST Pulldown Assay

All proteins were expressed in *E. coli* BL21(DE3) cells at 25°C by 0.3 mM isopropyl β-D-1-thiogalactopyranoside induction for 16 hr. Cells were harvested and lysed in PBS (Wako) or Tris-buffered saline (20 mM Tris-HCl, pH 9.0, 100 mM NaCl) including 1% Triton X-100 and immobilized onto GS4B (GE Healthcare) or Ni-NTA (Invitrogen), respectively. Immobilized proteins were cleaved with thrombin (GE Healthcare) at 22°C or 4°C for 16 hr. Eluted proteins were further purified by gel filtration (Superdex 200 10/300 GL; GE Healthcare). For GST pulldown assays, GST-fused LC3s and Atg13 deletion mutants were attached to GS4B and incubated with purified proteins for 1 hr at 4°C. After washing three times with PBS, the bound proteins were analyzed by SDS-PAGE followed by CBB staining.

Crystallization

Initial crystallization screening was performed using kits from Hampton Research (Crystal Screen and Crystal Screen 2, PEG/Ion Screen 1 and 2, MembFac and Index), from Emerald BioStructures (Wizard I and II, Cryo I and II), and from Molecular Dimensions (Stura Footprint Screens) by sitting-drop vapor diffusion method at 4°C and/or 20°C using an automatic crystallization robot system (Hiraki et al., 2006). The crystals of $LC3A^{2–121}$, $LC3C^{8–125}$, $Atg13^{436–447}$-$LC3A^{2–121}$, $Atg13^{436–447}$-$LC3B^{2–119}$, and $Atg13^{436–447}$-$LC3C^{8–125}$ were obtained using PEG/Ion Screen 2 condition No. 4 (0.2 M sodium malonate, pH 5.0, 20% [w/v] PEG3350) at 20°C, PEG/Ion Screen condition No. 48 (0.2 M di-ammonium hydrogen citrate, pH 5.1, 20% [w/v] PEG3350) at 4°C, MembFac condition No. 1 (0.1 M sodium acetate trihydrate, pH 4.6, 0.1 M sodium chloride, 12% [v/v] 2-methyl-2,4-pentanediol) at 4°C, Index condition No. 94 (0.2 M sodium citrate tribasic dihydrate, 20% [w/v] PEG3350) at 20°C, and Crystal Screen condition No. 37 (0.1 M sodium acetate trihydrate, pH 4.6, 8% [w/v] PEG4000) at 4°C, respectively. For crystallization of $LC3C^{8–125}$ and $Atg13^{436–447}$-$LC3B^{2–119}$, crystallization conditions were optimized manually by the hanging-drop vapor diffusion method. Finally, $LC3C^{8–125}$ proteins were crystallized using 0.5 M di-ammonium hydrogen citrate, pH 5.0, and 10% (w/v) PEG3350 at 4°C, and $Atg13^{436–447}$-$LC3B^{2–119}$ proteins were crystallized using 0.1 M sodium citrate tribasic dihydrate and 10% (w/v) PEG3350 at 4°C.

Data Collection, Structure Determination, Refinement, and Analyses

Diffraction data were collected at beamline BL-5A and BL-17A at Photon Factory. The crystals were mounted in nylon fiber loops and flash cooled in a nitrogen-gas stream. The diffraction data were indexed and integrated with Mosflm (Leslie and Powell, 2007) or XDS (Kabsch, 2010) and scaled with Scala (Collaborative Computational Project, Number 4, 1994). All crystal structures were solved by the molecular replacement method with the program MOLREP (Vagin and Teplyakov, 1997), using the structure of $LC3B^{2–119}$ as a search model (PDB code 3VTU). All models were refined with the programs CNS (Brünger et al., 1998) and REFMAC5 (Murshudov et al., 1997). Manual adjustments of the structure were performed with COOT (Emsley and Cowtan, 2004). All of the structural figures were generated with PyMOL (DeLano Scientific), and secondary structures were defined and assigned by the DSSP program (Kabsch and Sander, 1983).

SPR Measurement

Real-time binding analyses were performed using an SPR biosensor (Biacore 2000; GE Healthcare) at 25°C. Anti-GST antibodies were covalently coupled to a CM5 sensor chip (GE Healthcare) using a GST Capture Kit (GE Healthcare). For kinetic and interaction analyses, HBS-P (10 mM HEPES-NaOH, pH 7.4, 150 mM NaCl, 0.005% surfactant P20) was used as running buffer at a flow rate of 20 μl/min. GST and GST-Atg13 mutant proteins were diluted to 20 μg/ml in HBS-P and immobilized on a sensor chip for 180 s via anti-GST antibodies (flow cell 1 was immobilized with GST as a reference cell). LC3 proteins were injected using the Kinject program for 180 s. The sensor surface was regenerated by injecting 60 μl of 10 mM glysine-HCl, pH 2.1. The triplicate data were analyzed by the Scatchard plot (RU versus RU/concentration plot) and the K_D were calculated.

Autophagosome Formation Assay

MEFs were cultured in growth medium or Earle's balanced salt solution (Invitrogen) for 1 hr in the presence or absence of 100 nM Baf A1. MEFs expressing protein-fused GFP were directly observed with a confocal fluorescence microscope (FV1000; Olympus). The number of GFP-LC3A dots was determined by G-count (G-Angstrom). GFP-LC3A expression levels were checked by western blotting (Figure S7).

ACCESSION NUMBERS

The atomic coordinates and structure factors have been deposited in the Protein Data Bank with accession codes 3WAL, 3WAM, 3WAN, 3WAO, and 3WAP.

SUPPLEMENTAL INFORMATION

Supplemental Information includes seven figures and two tables and can be found with this article online at http://dx.doi.org/10.1016/j.str.2013.09.023.

ACKNOWLEDGMENTS

This work was supported by the Researcher Exchange Program between JSPS and RSNZ to H.S. (FY2012). R.C.J.D. acknowledges the following for funding support, in part: (1) the Ministry of Business, Innovation and Employment (contract UOCX1208), (2) the New Zealand Royal Society Marsden Fund (contract UOC1013), and (3) the U.S. Army Research Laboratory and U.S. Army Research Office under contract/grant number W911NF-11-1-0481.

Received: May 28, 2013
Revised: September 1, 2013
Accepted: September 24, 2013
Published: November 27, 2013

REFERENCES

Alemu, E.A., Lamark, T., Torgersen, K.M., Birgisdottir, A.B., Larsen, K.B., Jain, A., Olsvik, H., Øvervatn, A., Kirkin, V., and Johansen, T. (2012). ATG8 family proteins act as scaffolds for assembly of the ULK complex: sequence requirements for LC3-interacting region (LIR) motifs. J. Biol. Chem. *287*, 39275–39290.

Bajorek, M., Morita, E., Skalicky, J.J., Morham, S.G., Babst, M., and Sundquist, W.I. (2009). Biochemical analyses of human IST1 and its function in cytokinesis. Mol. Biol. Cell *20*, 1360–1373.

Bavro, V.N., Sola, M., Bracher, A., Kneussel, M., Betz, H., and Weissenhorn, W. (2002). Crystal structure of the GABA(A)-receptor-associated protein, GABARAP. EMBO Rep. *3*, 183–189.

Brünger, A.T., Adams, P.D., Clore, G.M., DeLano, W.L., Gros, P., Grosse-Kunstleve, R.W., Jiang, J.S., Kuszewski, J., Nilges, M., Pannu, N.S., et al. (1998). Crystallography & NMR system: a new software suite for macromolecular structure determination. Acta Crystallogr. D Biol. Crystallogr. *54*, 905–921.

Chan, E.Y., Kir, S., and Tooze, S.A. (2007). siRNA screening of the kinome identifies ULK1 as a multidomain modulator of autophagy. J. Biol. Chem. *282*, 25464–25474.

Chan, E.Y., Longatti, A., McKnight, N.C., and Tooze, S.A. (2009). Kinase-inactivated ULK proteins inhibit autophagy via their conserved C-terminal domains using an Atg13-independent mechanism. Mol. Cell. Biol. *29*, 157–171.

Collaborative Computational Project, Number 4. (1994). The CCP4 suite: programs for protein crystallography. Acta Crystallogr. D Biol. Crystallogr. *50*, 760–763.

Dikic, I., Johansen, T., and Kirkin, V. (2010). Selective autophagy in cancer development and therapy. Cancer Res. *70*, 3431–3434.

Durocher, Y., Perret, S., and Kamen, A. (2002). High-level and high-throughput recombinant protein production by transient transfection of suspension-growing human 293-EBNA1 cells. Nucleic Acids Res. *30*, E9.

Emsley, P., and Cowtan, K. (2004). Coot: model-building tools for molecular graphics. Acta Crystallogr. D Biol. Crystallogr. *60*, 2126–2132.

Funakoshi, T., Matsuura, A., Noda, T., and Ohsumi, Y. (1997). Analyses of APG13 gene involved in autophagy in yeast, *Saccharomyces cerevisiae*. Gene *192*, 207–213.

Hara, T., Takamura, A., Kishi, C., Iemura, S., Natsume, T., Guan, J.L., and Mizushima, N. (2008). FIP200, a ULK-interacting protein, is required for autophagosome formation in mammalian cells. J. Cell Biol. *181*, 497–510.

He, H., Dang, Y., Dai, F., Guo, Z., Wu, J., She, X., Pei, Y., Chen, Y., Ling, W., Wu, C., et al. (2003). Post-translational modifications of three members of the human MAP1LC3 family and detection of a novel type of modification for MAP1LC3B. J. Biol. Chem. *278*, 29278–29287.

Hemelaar, J., Lelyveld, V.S., Kessler, B.M., and Ploegh, H.L. (2003). A single protease, Apg4B, is specific for the autophagy-related ubiquitin-like proteins GATE-16, MAP1-LC3, GABARAP, and Apg8L. J. Biol. Chem. *278*, 51841–51850.

Hiraki, M., Kato, R., Nagai, M., Satoh, T., Hirano, S., Ihara, K., Kudo, N., Nagae, M., Kobayashi, M., Inoue, M., et al. (2006). Development of an automated large-scale protein-crystallization and monitoring system for high-throughput protein-structure analyses. Acta Crystallogr. D Biol. Crystallogr. *62*, 1058–1065.

Hosokawa, N., Sasaki, T., Iemura, S., Natsume, T., Hara, T., and Mizushima, N. (2009). Atg101, a novel mammalian autophagy protein interacting with Atg13. Autophagy *5*, 973–979.

Ichimura, Y., and Komatsu, M. (2010). Selective degradation of p62 by autophagy. Semin. Immunopathol. *32*, 431–436.

Ichimura, Y., Kumanomidou, T., Sou, Y.S., Mizushima, T., Ezaki, J., Ueno, T., Kominami, E., Yamane, T., Tanaka, K., and Komatsu, M. (2008). Structural basis for sorting mechanism of p62 in selective autophagy. J. Biol. Chem. *283*, 22847–22857.

Johansen, T., and Lamark, T. (2011). Selective autophagy mediated by autophagic adapter proteins. Autophagy *7*, 279–296.

Kabeya, Y., Kawamata, T., Suzuki, K., and Ohsumi, Y. (2007). Cis1/Atg31 is required for autophagosome formation in *Saccharomyces cerevisiae*. Biochem. Biophys. Res. Commun. *356*, 405–410.

Kabsch, W. (2010). XDS. Acta Crystallogr. D Biol. Crystallogr. *66*, 125–132.

Kabsch, W., and Sander, C. (1983). Dictionary of protein secondary structure: pattern recognition of hydrogen-bonded and geometrical features. Biopolymers *22*, 2577–2637.

Kamada, Y., Funakoshi, T., Shintani, T., Nagano, K., Ohsumi, M., and Ohsumi, Y. (2000). Tor-mediated induction of autophagy via an Apg1 protein kinase complex. J. Cell Biol. *150*, 1507–1513.

Kawamata, T., Kamada, Y., Suzuki, K., Kuboshima, N., Akimatsu, H., Ota, S., Ohsumi, M., and Ohsumi, Y. (2005). Characterization of a novel autophagy-specific gene, ATG29. Biochem. Biophys. Res. Commun. *338*, 1884–1889.

Kraft, C., Kijanska, M., Kalie, E., Siergiejuk, E., Lee, S.S., Semplicio, G., Stoffel, I., Brezovich, A., Verma, M., Hansmann, I., et al. (2012). Binding of the Atg1/ULK1 kinase to the ubiquitin-like protein Atg8 regulates autophagy. EMBO J. *31*, 3691–3703.

Kumeta, H., Watanabe, M., Nakatogawa, H., Yamaguchi, M., Ogura, K., Adachi, W., Fujioka, Y., Noda, N.N., Ohsumi, Y., and Inagaki, F. (2010). The NMR structure of the autophagy-related protein Atg8. J. Biomol. NMR *47*, 237–241.

Larkin, M.A., Blackshields, G., Brown, N.P., Chenna, R., McGettigan, P.A., McWilliam, H., Valentin, F., Wallace, I.M., Wilm, A., Lopez, R., et al. (2007). Clustal W and Clustal X version 2.0. Bioinformatics *23*, 2947–2948.

Leslie, A.G.W., and Powell, H.R. (2007). Processing diffraction data with mosflm. In Evolving Methods for Macromolecular Crystallography, R.J. Read and J.L. Sussman, eds. (Dordrecht: Springer), pp. 41–51.

Levine, B., and Kroemer, G. (2008). Autophagy in the pathogenesis of disease. Cell *132*, 27–42.

Li, M., Hou, Y., Wang, J., Chen, X., Shao, Z.M., and Yin, X.M. (2011). Kinetics comparisons of mammalian Atg4 homologues indicate selective preferences toward diverse Atg8 substrates. J. Biol. Chem. *286*, 7327–7338.

Madaule, P., Eda, M., Watanabe, N., Fujisawa, K., Matsuoka, T., Bito, H., Ishizaki, T., and Narumiya, S. (1998). Role of citron kinase as a target of the small GTPase Rho in cytokinesis. Nature *394*, 491–494.

Mizushima, N., Levine, B., Cuervo, A.M., and Klionsky, D.J. (2008). Autophagy fights disease through cellular self-digestion. Nature *451*, 1069–1075.

Murshudov, G.N., Vagin, A.A., and Dodson, E.J. (1997). Refinement of macromolecular structures by the maximum-likelihood method. Acta Crystallogr. D Biol. Crystallogr. *53*, 240–255.

Nakatogawa, H., Ichimura, Y., and Ohsumi, Y. (2007). Atg8, a ubiquitin-like protein required for autophagosome formation, mediates membrane tethering and hemifusion. Cell *130*, 165–178.

Noda, N.N., Kumeta, H., Nakatogawa, H., Satoo, K., Adachi, W., Ishii, J., Fujioka, Y., Ohsumi, Y., and Inagaki, F. (2008). Structural basis of target recognition by Atg8/LC3 during selective autophagy. Genes Cells *13*, 1211–1218.

Noda, N.N., Ohsumi, Y., and Inagaki, F. (2010). Atg8-family interacting motif crucial for selective autophagy. FEBS Lett. *584*, 1379–1385.

Paz, Y., Elazar, Z., and Fass, D. (2000). Structure of GATE-16, membrane transport modulator and mammalian ortholog of autophagocytosis factor Aut7p. J. Biol. Chem. *275*, 25445–25450.

Rogov, V.V., Suzuki, H., Fiskin, E., Wild, P., Kniss, A., Rozenknop, A., Kato, R., Kawasaki, M., McEwan, D.G., Löhr, F., et al. (2013). Structural basis for phosphorylation-triggered autophagic clearance of Salmonella. Biochem. J. *454*, 459–466.

Rozenknop, A., Rogov, V.V., Rogova, N.Y., Löhr, F., Güntert, P., Dikic, I., and Dötsch, V. (2011). Characterization of the interaction of GABARAPL-1 with the LIR motif of NBR1. J. Mol. Biol. *410*, 477–487.

Satoo, K., Noda, N.N., Kumeta, H., Fujioka, Y., Mizushima, N., Ohsumi, Y., and Inagaki, F. (2009). The structure of Atg4B-LC3 complex reveals the mechanism of LC3 processing and delipidation during autophagy. EMBO J. *28*, 1341–1350.

Schlumpberger, M., Schaeffeler, E., Straub, M., Bredschneider, M., Wolf, D.H., and Thumm, M. (1997). AUT1, a gene essential for autophagocytosis in the yeast *Saccharomyces cerevisiae*. J. Bacteriol. *179*, 1068–1076.

Sugawara, K., Suzuki, N.N., Fujioka, Y., Mizushima, N., Ohsumi, Y., and Inagaki, F. (2004). The crystal structure of microtubule-associated protein light chain 3, a mammalian homologue of *Saccharomyces cerevisiae* Atg8. Genes Cells *9*, 611–618.

Taherbhoy, A.M., Tait, S.W., Kaiser, S.E., Williams, A.H., Deng, A., Nourse, A., Hammel, M., Kurinov, I., Rock, C.O., Green, D.R., and Schulman, B.A. (2011). Atg8 transfer from Atg7 to Atg3: a distinctive E1-E2 architecture and mechanism in the autophagy pathway. Mol. Cell *44*, 451–461.

Tanida, I., Mizushima, N., Kiyooka, M., Ohsumi, M., Ueno, T., Ohsumi, Y., and Kominami, E. (1999). Apg7p/Cvt2p: a novel protein-activating enzyme essential for autophagy. Mol. Biol. Cell *10*, 1367–1379.

Tanida, I., Sou, Y.S., Ezaki, J., Minematsu-Ikeguchi, N., Ueno, T., and Kominami, E. (2004). HsAtg4B/HsApg4B/autophagin-1 cleaves the carboxyl termini of three human Atg8 homologues and delipidates microtubule-associated protein light chain 3- and GABAA receptor-associated protein-phospholipid conjugates. J. Biol. Chem. *279*, 36268–36276.

Vagin, A., and Teplyakov, A. (1997). MOLREP: an automated program for molecular replacement. J. Appl. Crystallogr. *30*, 1022–1025.

von Muhlinen, N., Akutsu, M., Ravenhill, B.J., Foeglein, Á., Bloor, S., Rutherford, T.J., Freund, S.M., Komander, D., and Randow, F. (2012). LC3C, bound selectively by a noncanonical LIR motif in NDP52, is required for antibacterial autophagy. Mol. Cell *48*, 329–342.

Weiergräber, O.H., Stangler, T., Thielmann, Y., Mohrlüder, J., Wiesehan, K., and Willbold, D. (2008). Ligand binding mode of GABAA receptor-associated protein. J. Mol. Biol. *381*, 1320–1331.

Wild, P., Farhan, H., McEwan, D.G., Wagner, S., Rogov, V.V., Brady, N.R., Richter, B., Korac, J., Waidmann, O., Choudhary, C., et al. (2011). Phosphorylation of the autophagy receptor optineurin restricts Salmonella growth. Science *333*, 228–233.

Xin, Y., Yu, L., Chen, Z., Zheng, L., Fu, Q., Jiang, J., Zhang, P., Gong, R., and Zhao, S. (2001). Cloning, expression patterns, and chromosome localization of three human and two mouse homologues of GABA(A) receptor-associated protein. Genomics *74*, 408–413.

Published October 7, 2013

Recruitment of the autophagic machinery to endosomes during infection is mediated by ubiquitin

Naonobu Fujita,[1,2] Eiji Morita,[3] Takashi Itoh,[8] Atsushi Tanaka,[2] Megumi Nakaoka,[2] Yuki Osada,[1] Tetsuo Umemoto,[2] Tatsuya Saitoh,[4,5] Hitoshi Nakatogawa,[7] Shouhei Kobayashi,[9] Tokuko Haraguchi,[9] Jun-Lin Guan,[10] Kazuhiro Iwai,[11] Fuminori Tokunaga,[12] Kazunobu Saito,[6] Koutaro Ishibashi,[8] Shizuo Akira,[4,5] Mitsunori Fukuda,[8] Takeshi Noda,[1,2] and Tamotsu Yoshimori[1,2]

[1]Department of Genetics, Graduate School of Medicine, [2]Laboratory of Intracellular Membrane Dynamics, Graduate school of Frontier Biosciences, [3]Department of Molecular Virology, Research Institute for Microbial Diseases, [4]Department of Host Defense, WPI Immunology Frontier Research Center, [5]Department of Host Defense, Research Institute for Microbial Disease, and [6]Core Instrumentation Facility, Research Institute for Microbial Disease, Osaka University, 2-2 Yamadaoka, Suita, Osaka 565-0871, Japan
[7]Frontier Research Center, Tokyo Institute of Technology, Yokohama 226-8503, Japan
[8]Department of Developmental Biology and Neurosciences, Graduate School of Life Sciences, Tohoku University, Sendai, Miyagi 980-8578, Japan
[9]Advance ICT Research Institute Kobe, National Institute of Information and Communications Technology, Kobe 651-2492, Japan
[10]Department of Internal Medicine–MMG, University of Michigan Medical School, Ann Arbor, MI 48109
[11]Department of Molecular and Cellular Physiology, Graduate School of Medicine, Kyoto University, Yoshida-konoe-cho, Sakyo-ku, Kyoto 606-8501, Japan
[12]Institute for Molecular and Cellular Regulation, Gunma University, 3-39-15 Showa-machi, Maebashi, Gunma 371-8512, Japan

Although ubiquitin is thought to be important for the autophagic sequestration of invading bacteria (also called xenophagy), its precise role remains largely enigmatic. Here we determined how ubiquitin is involved in this process. After invasion, ubiquitin is conjugated to host cellular proteins in endosomes that contain *Salmonella* or transfection reagent–coated latex (polystyrene) beads, which mimic invading bacteria. Ubiquitin is recognized by the autophagic machinery independently of the LC3–ubiquitin interaction through adaptor proteins, including a direct interaction between ubiquitin and Atg16L1. To ensure that invading pathogens are captured and degraded, Atg16L1 targeting is secured by two backup systems that anchor Atg16L1 to ubiquitin-decorated endosomes. Thus, we reveal that ubiquitin is a pivotal molecule that connects bacteria-containing endosomes with the autophagic machinery upstream of LC3.

Introduction

Autophagy is a membrane trafficking process in which double membrane–bound spherical structures called autophagosomes deliver cytosolic contents to lysosomes/vacuoles for degradation. In addition to the well-understood physiological role of autophagy in recycling intracellular materials in response to starvation, there is increasing evidence that autophagy is involved in diverse physiological processes such as cellular immunity. Autophagy specifically targets invading bacteria to restrict their growth (also called xenophagy; Mizushima et al., 2008).

Autophagosome formation is mediated by at least 18 core autophagy-related (Atg) proteins, which comprise the following six functional units (Suzuki and Ohsumi, 2010): (1) the uncoordinated 51-like kinase (ULK)–Atg1 protein kinase complex, (2) the autophagy-specific phosphatidylinositol 3-kinase (PI3K) complex, (3) the phosphatidylinositol 3-phosphate (PI3P)–binding protein complex, (4) Atg9L1, (5) the LC3 (mammalian homologue of yeast Atg8) system, and (6) the Atg12 system. Two ubiquitin (Ub)-like molecules, LC3 and Atg12, are covalently conjugated to phosphatidylethanolamine (PE) and Atg5, respectively. The Atg12–Atg5 conjugate associates with Atg16L1 to form a dimeric complex (referred to as the Atg16L1 complex; Mizushima et al., 2003; Fujita et al., 2009), and functions as an E3-like factor in the LC3 system (Fujita et al., 2008b). ULK1

N. Fujita and E. Morita contributed equally to this paper.

Correspondence to Tamotsu Yoshimori: tamyoshi@fbs.osaka-u.ac.jp; or Takeshi Noda: takenoda@dent.osaka-u.ac.jp

N. Fujita's present address is Division of Biological Sciences, University of California, San Diego, La Jolla, CA 92093.

T. Noda's present address is Graduate School of Dentistry, Osaka University, Osaka 565-0871, Japan.

Abbreviations used in this paper: EBSS, Earle's balanced salt solution; FIP200, FAK family-interacting protein of 200 kD; MEF, mouse embryonic fibroblast; PE, phosphatidylethanolamine; *Salmonella*, *Salmonella enterica* serovar Typhimurium; Ub, ubiquitin; ULK, uncoordinated 51-like kinase.

Supplemental Material can be found at:
http://jcb.rupress.org/content/suppl/2013/10/02/jcb.201304188.DC1.html

The Rockefeller University Press $30.00
J. Cell Biol. Vol. 203 No. 1 115–128
www.jcb.org/cgi/doi/10.1083/jcb.201304188

Published October 7, 2013

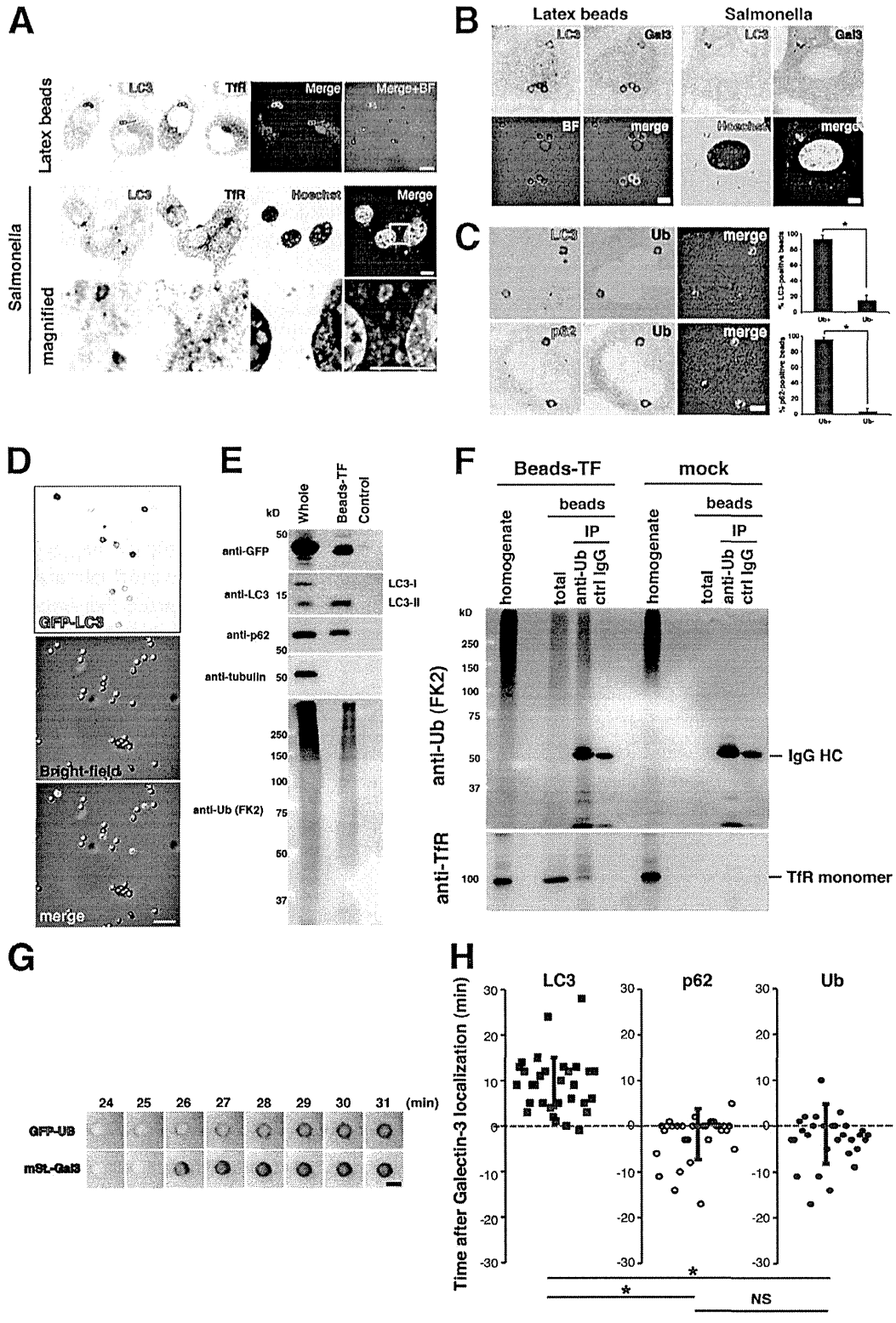

Figure 1. **Ub-positive endosomes containing *Salmonella* or beads are targeted by autophagy.** (A) HeLa cells were infected with *S.* Typhimurium (*Salmonella*) for 1 h or transfected with Effectene-coated latex beads for 3 h and then subjected to immunocytochemistry for LC3 and transferrin receptor (TfR). Bar, 10 µm. (B) HeLa cells were infected with *Salmonella* for 1 h or transfected with Effectene-coated latex beads for 3 h and then subjected to immunocytochemistry for LC3 and galectin3. Bar, 5 µm. (C) HeLa cells were transfected with Effectene-coated latex beads for 3 h and subjected to immunocytochemistry for LC3 and Ub (top) or LC3 and p62 (bottom). Bar, 5 µm. The percentages of LC3- or p62-positive beads per Ub-positive (Ub+) or Ub-negative (Ub−) beads were

Published October 7, 2013

and ULK2, the mammalian homologues of yeast Atg1, are serine/threonine protein kinases that form a large protein complex with Atg13, a FAK family-interacting protein of 200 kD (FIP200), and Atg101 (referred to as the ULK1 complex; Mizushima, 2010). The ULK1 complex plays an essential role in initiating autophagosome formation (Mizushima, 2010).

Ubiquitination is thought to play important roles during xenophagy because LC3-positive bacteria are also decorated with Ub. However, it is largely unknown how Ub contributes to the autophagic response against invading bacteria (Fujita and Yoshimori, 2011). Furthermore, the target of ubiquitination is unknown, although plausible candidates are bacterial surface proteins.

How Ub is linked to autophagosome formation is still problematic, although it is widely accepted that adaptor proteins bridge ubiquitinated substrates and autophagosomal membranes by binding to both Ub and LC3, which localizes to autophagosomal membranes. The adaptors p62, NDP52, and optineurin possess both a Ub-binding domain and LC3-binding domain and are required for efficient selective autophagy against bacteria (Thurston et al., 2009; Yoshikawa et al., 2009; Zheng et al., 2009; Wild et al., 2011). However, it is still debated whether the selectivity in autophagy against bacteria is attributed only to LC3–adaptor interactions. We recently reported that the LC3 system is dispensable to localize other Atg proteins and to form the autophagic double membrane in response to invading bacteria (Kageyama et al., 2011). These findings suggest that the selectivity of autophagy is not accounted for by the interaction between adaptors and LC3 and other mechanisms that recruit other Atgs could be responsible for Ub selectivity. We also confirmed that both LC3 lipidation, which is required for autophagosome binding, and LC3 recruitment to the target depend on recruitment of the Atg16L1 complex, even if adaptors exist (Kageyama et al., 2011).

In this study, we propose a novel model for autophagy against bacteria using *Salmonella enterica* serovar Typhimurium (*S.* Typhimurium or *Salmonella*) and transfection reagent–coated latex beads as model substrates (Kobayashi et al., 2010). The ubiquitination of host proteins within bacteria- or bead-containing endosomes plays a role in induction of selective autophagy. Furthermore, we show that Atg16L1, one of the earliest recruited and upstream Atgs, both directly and indirectly recognizes the Ub-decorated endosomes through multiple pathways.

Results

Proteins on bead- or *Salmonella*-containing endosomes are ubiquitinated

It was previously suggested that *Salmonella enterica* serovar Typhimurium (*S.* Typhimurium) is targeted by autophagy before escaping from endosomes. (Birmingham and Brumell, 2006; Zheng et al., 2009; Kageyama et al., 2011; Thurston et al., 2012). In addition, it has been recently reported that polystyrene beads coated with transfection reagents are selectively targeted by LC3-positive autophagosomes after being endocytosed into cells, although uncoated beads are not sequestered by autophagy even if internalized into endosomes (Kobayashi et al., 2010). Presumably, damage of endosomes by transfection reagents triggers autophagy. Because LC3 colocalized with transferrin receptor in both *Salmonella*-infected and bead-transfected cells (Fig. 1 A), both *Salmonella* and the beads are targeted by autophagy while within endosomes. Furthermore, LC3-positve *Salmonella* and beads were galectin3-positive (Fig. 1 B). Galectin3 is a β-galactose–binding lectin and a good marker of damaged endosomes because the lumenal glycochain becomes accessible to cytosolic galectin3 (Paz et al., 2010). These results suggest that autophagosomes form in response to *Salmonella*- or bead-containing endosomes whose membranes are broken and permeabilized, perhaps by the *Salmonella* type III secretion system or transfection reagents, respectively. In addition, Ub clearly surrounded the LC3-positive or p62-positive transfected beads in the same manner as during autophagy against invading bacteria (Fig. 1 C; Yoshikawa et al., 2009; Zheng et al., 2009).

To examine the targets of ubiquitination, we purified beads surrounded by autophagosomal membranes using density gradient centrifugation (Fig. 1 D). As a result, ubiquitinated proteins were detected in the bead-containing autophagosome fraction, which contains lipidated LC3 and p62 (Fig. 1 E). Because the artificial latex beads do not have any proteins on their surface, host cellular proteins must be ubiquitinated in the process. The most plausible ubiquitinated targets are endosomal proteins because autophagosomes sequester the beads within endosomes. In fact, the purified bead–autophagosome fraction contained ubiquitinated transferrin receptor, which is not typically ubiquitinated because it is a recycling receptor (Fig. 1 F). We reasoned that any endosomal protein could be a ubiquitination target. From these results, we conclude that endosomal membranes, which are damaged by the bacteria or beads within the endosomes, are ubiquitinated and targeted by autophagy.

We next asked the order of events among endosomal rupture, ubiquitination, and LC3 recruitment using dual-color live-cell imaging analysis. Ub appeared around the transfected beads nearly concomitantly with galectin3. p62 also appeared together with galectin3. By contrast, LC3 was always recruited after galectin3, and localized around the beads 0–15 min after galectin3 (Fig. 1, G and H; Videos 1 and 2; and unpublished data). Presumably, endosomal rupture rapidly triggers the ubiquitination of intrinsic proteins, after which LC3 is slowly recruited to the endosomes.

enumerated. Statistical analysis was performed by Student's unpaired *t* test. *, $P < 0.01$. (D and E) HeLa cells stably expressing GFP-LC3 were transfected with Effectene-coated latex beads for 3 h. Bead–autophagosomes were fractionated as described in Materials and methods. The bead–autophagosome fraction was observed by confocal microscopy (D; bar, 10 µm) or lysed with RIPA buffer and subjected to Western blot analysis using the indicated antibodies (E). In a control sample, scraped cells were mixed with Effectene-coated beads and immediately homogenized. (F) The bead–autophagosome fraction was lysed and subjected to immunoprecipitation with an anti-Ub IgG antibody (FK2) or control IgG. Co-immunoprecipitated molecules were examined by Western blotting using the indicated antibodies. (G and H) NIH3T3 cells stably expressing mStrawberry (mStr)-Gal3 and GFP-LC3, mStr-Gal3, and GFP-p62, or mStr-Gal3 and GFP-Ub were transfected with Effectene-coated latex beads for 30 min and then washed. Live cells were observed at 1-min intervals by fluorescence microscopy. Bar, 3 µm. The time after galectin3 localization was measured for at least 30 cases for each combination (H). Statistical analysis was performed by Student's unpaired *t* test. *, $P < 0.05$; NS, not significant.

Published October 7, 2013

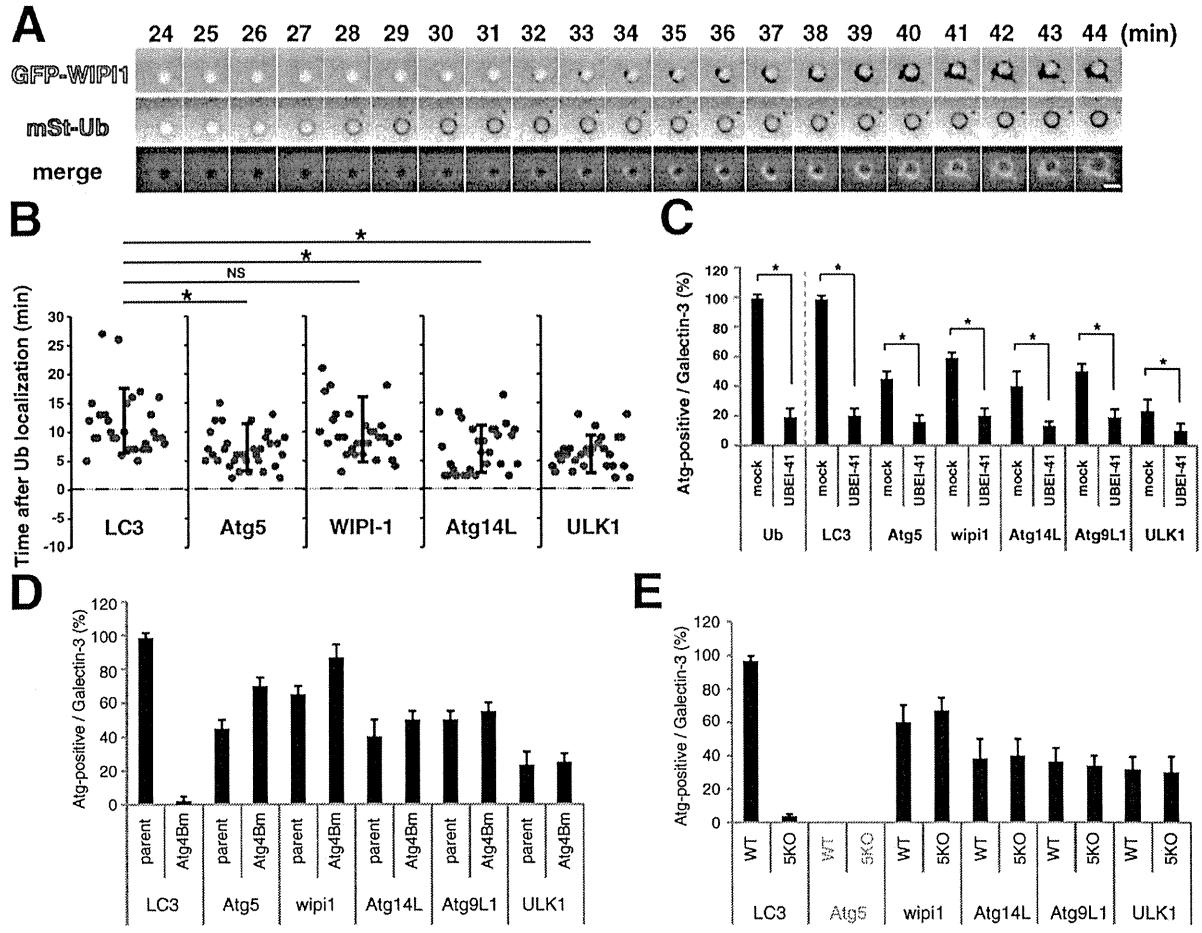

Figure 2. **Ubiquitination and recruitment of Atg proteins.** (A and B) NIH3T3 cells stably expressing mStr-Ub and GFP-tagged LC3, Atg5, WIPI-1, Atg14L1, or ULK1 were transfected with Effectene-coated latex beads for 30 min. Then, live cells were observed at 1-min intervals by fluorescence microscopy. Bar, 3 µm. The time after Ub localization was measured for at least 30 cases for each combination. Each value represents the mean ± SD. Statistical analysis was performed by Student's unpaired *t* test. *, $P < 0.05$; NS, not significant. (C) NIH3T3 cells stably expressing GFP-tagged Ub, LC3, Atg5, WIPI-1, Atg14L1, Atg9L1, or ULK1 were transfected with Effectene-coated beads for 3 h in the presence or absence (mock) of 30 µM UBEI-41 (a ubiquitin E1–specific inhibitor) and subjected to immunocytochemistry for galectin3. The percentages of GFP-positive per galectin3-positive beads were enumerated. At least 30 beads were counted ($n = 3$). The values are the mean ± SD. Statistical analysis was performed by Student's unpaired *t* test. *, $P < 0.05$. (D and E) Parent NIH3T3 cells, Atg4B mutant overexpressing NIH3T3 cells (D), wild-type MEFs, and Atg5-KO MEFs (E) stably expressing GFP-tagged LC3, Atg5, WIPI-1, Atg14L1, Atg9L1, or ULK1 were transfected with Effectene-coated latex beads for 3 h and subjected to immunocytochemistry for galectin3. The percentages of Atg-positive per galectin3-positive beads were enumerated. At least 30 beads were counted ($n = 3$). The values are the mean ± SD.

Ubiquitination is required to recruit Atg proteins

To determine the order in which Ub as well as LC3 and other Atg proteins are recruited to the transfected beads, we performed live-cell imaging of bead-transfected NIH3T3 cells stably expressing mStr-tagged Ub and the GFP-tagged Atg proteins LC3, Atg5, WIPI1, Atg14L, and ULK1 (Fig. 2, A and B; and Videos 3–7). The trafficking of each Atg protein greatly differed (Videos 3–7). The time lag between the localization of each Atg protein and Ub was quantified (Fig. 2 B). All of the Atg proteins were recruited to the transfected beads after Ub recruitment. Remarkably, LC3 and WIPI1 localized to the beads after the other Atg proteins, suggesting that the autophagic machinery recognizes the ubiquitinated substrate independently of an LC3-mediated mechanism.

Next, to directly demonstrate the necessity of ubiquitination, we used a Ub-activating enzyme (E1)–specific inhibitor (UBEI-41) because it enables blockade of ubiquitination instantly in cultured cells (Yang et al., 2007). As expected, the number of Ub-positive beads among galectin3-positive beads was drastically reduced upon UBEI-41 treatment (Fig. 2 C, Ub). Galectin3 was recruited to transfected beads even in UBEI-treated cells, indicating that internalization of beads and endosomal rupture occurred in our experimental condition. We also found that administering UBEI-41 strongly inhibited LC3 recruitment (Fig. 2 C, LC3). Moreover, the localization of all of the other representative Atg proteins was severely affected by UBEI-41 treatment. These results indicate that ubiquitination plays an important role in recruiting not only LC3 but also other Atg proteins to invading pathogens.

Published October 7, 2013

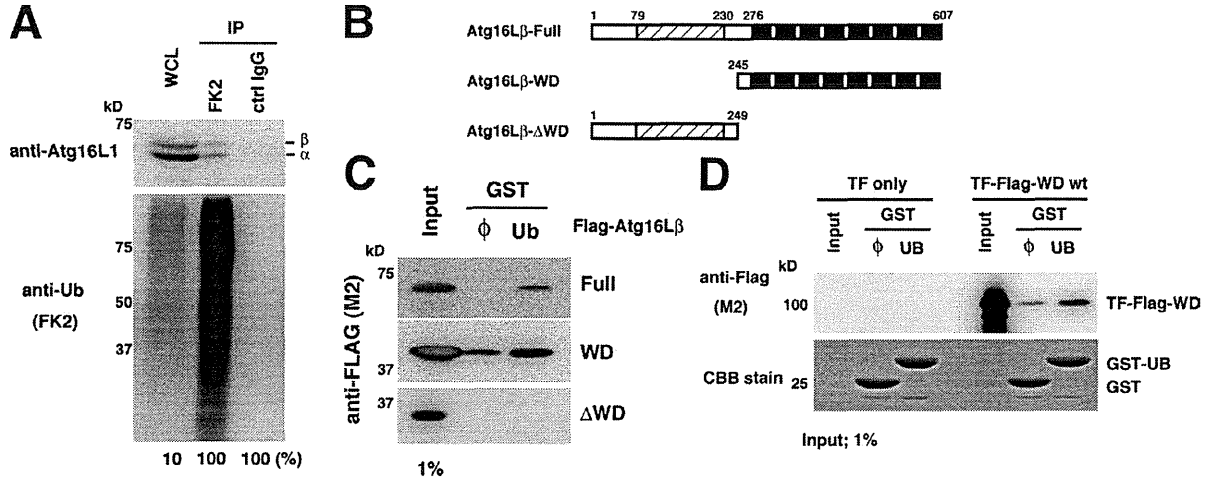

Figure 3. **The WD β-propellers of Atg16L1 directly interact with Ub.** (A) HeLa cells were lysed with 1% Triton X-100 lysis buffer and subjected to immunoprecipitation with FK2- or control IgG-immobilized beads. The coimmunoprecipitated molecules were examined by Western blotting using the indicated antibodies. (B) Schematic diagram of Atg16L1 (Full) and its deletion constructs. (C) Purified recombinant GST or GST-Ub–immobilized glutathione Sepharose beads were incubated with lysates from HEK293T cells transiently expressing FLAG-tagged Atg16L1 constructs for 1 h at 25°C with gentle agitation. The beads were washed three times with ice-cold PBS and the bound complexes were eluted with 50 mM reduced glutathione and then subjected to Western blotting for FLAG. (D) Purified GST or GST-Ub–immobilized glutathione Sepharose beads were incubated with lysates from bacteria expressing trigger factor (TF) or TF-FLAG-WD β-propellers for 1 h at 25°C with gentle agitation. Washing and elution were performed as described in C. The eluted samples were subjected to SDS-PAGE and Western blotting for FLAG.

Likewise, we systematically quantified the recruitment of Atg proteins to galectin3-positive structures in autophagy-deficient cells (Atg5-KO, Atg14L-KO, Atg9L1-KO, and FIP200-KO cells as well as cells expressing an Atg4B mutant in which the LC3 system is blocked) stably expressing a series of GFP-tagged Atg proteins (Fig. 2, D and E; and Fig. S1; Kuma et al., 2004; Fujita et al., 2008a; Hara and Mizushima, 2009; Matsunaga et al., 2009; Saitoh et al., 2009). The ULK1 complex, Atg9L1, and the Atg16L1 complex were recruited to galectin3-positive structures independently of other Atg proteins (Fig. 2, D and E; and Fig. S1), which is consistent with autophagy against *Salmonella* and Parkin-mediated mitophagy (Itakura et al., 2012; Kageyama et al., 2011), and our live-cell imaging data (Fig. 2, A and B). Altogether, it is clear that before LC3 recruitment, the three core autophagy machineries, notably the Atg16L1 complex, the ULK1 complex, and Atg9L1, independently recognize the ubiquitinated endosomes containing bacteria or beads.

Ub moieties vary from mono-Ub to extended chains, linked through seven lysine residues in Ub or via the N-terminal methionine residue (linear; Iwai and Tokunaga, 2009). It has been recently reported that K63- and linear-linked Ub chains clearly colocalize with invading *Salmonella* (van Wijk et al., 2012). To examine the presence of K48- and K63-linked Ub chains to the invading *Salmonella* or transfected beads, we used K48- or K63-specific antibodies (Newton et al., 2008). Both K48- and K63-linked Ub signals were well colocalized with poly-Ub signals (Fig. S2 A). This result and the previous report show that different Ub linkages, including K48, K63, and linear, could be part of the Ub coat on the invading *Salmonella* and transfected beads.

It remains enigmatic which linkage of Ub is required for selective autophagy. To test loss of function of K63-linked or linear-linked Ub chains, Ubc13$^{f/f}$, HOIL-1L KO, and their control mouse embryonic fibroblasts (MEFs) were challenged with *Salmonella* (Yamamoto et al., 2006; Tokunaga et al., 2009). Ubc13 is an E2 enzyme crucial for generating K63-linked chains (Hofmann and Pickart, 1999), and HOIL-1L is an accessory protein of the LUBAC E3 ligase complex that is very important for efficient formation of linear-linked Ub chains (Tokunaga et al., 2009). We found that neither Ubc13$^{f/f}$ nor HOIL-1L KO blocked LC3 recruitment to the Ub-positive *Salmonella* (Fig. S2, B and C). Collectively, these results indicate that autophagic machinery targeting did not depend solely on K63- or linear-Ub linkages.

The WD β-propellers of Atg16L1 directly interact with Ub

How do the three core autophagy machineries recognize the Ub-positive substrate? We focused on Atg16L1 because it contains a C-terminal WD β-propeller domain, whose function is unknown, but the same domain in several other proteins reportedly functions as an Ub-binding domain (Pashkova et al., 2010). Therefore, we tested the possibility that Ub directly interacts with the WD β-propellers of Atg16L1. First, we examined whether endogenous Atg16L1 coimmunoprecipitated with polyubiquitinated proteins. As shown in Fig. 3 A, Atg16L1 was detected in FK2 (a monoclonal antibody against poly Ub)-immunoprecipitated samples, but not in a control sample immunoprecipitated with IgG. To examine the interaction more directly, a GST pull-down experiment was performed. Purified GST or GST-Ub was immobilized to glutathione Sepharose beads (Fig. S3 A) and incubated with lysates of HEK293T cells transiently expressing a series of FLAG-tagged Atg16L1 constructs, including full-length Atg16L1, the WD β-propellers alone, or Atg16L1 lacking the complete WD region (ΔWD; Fig. 3 B). Full-length and the WD β-propellers bound to GST-Ub more efficiently than to

Published October 7, 2013

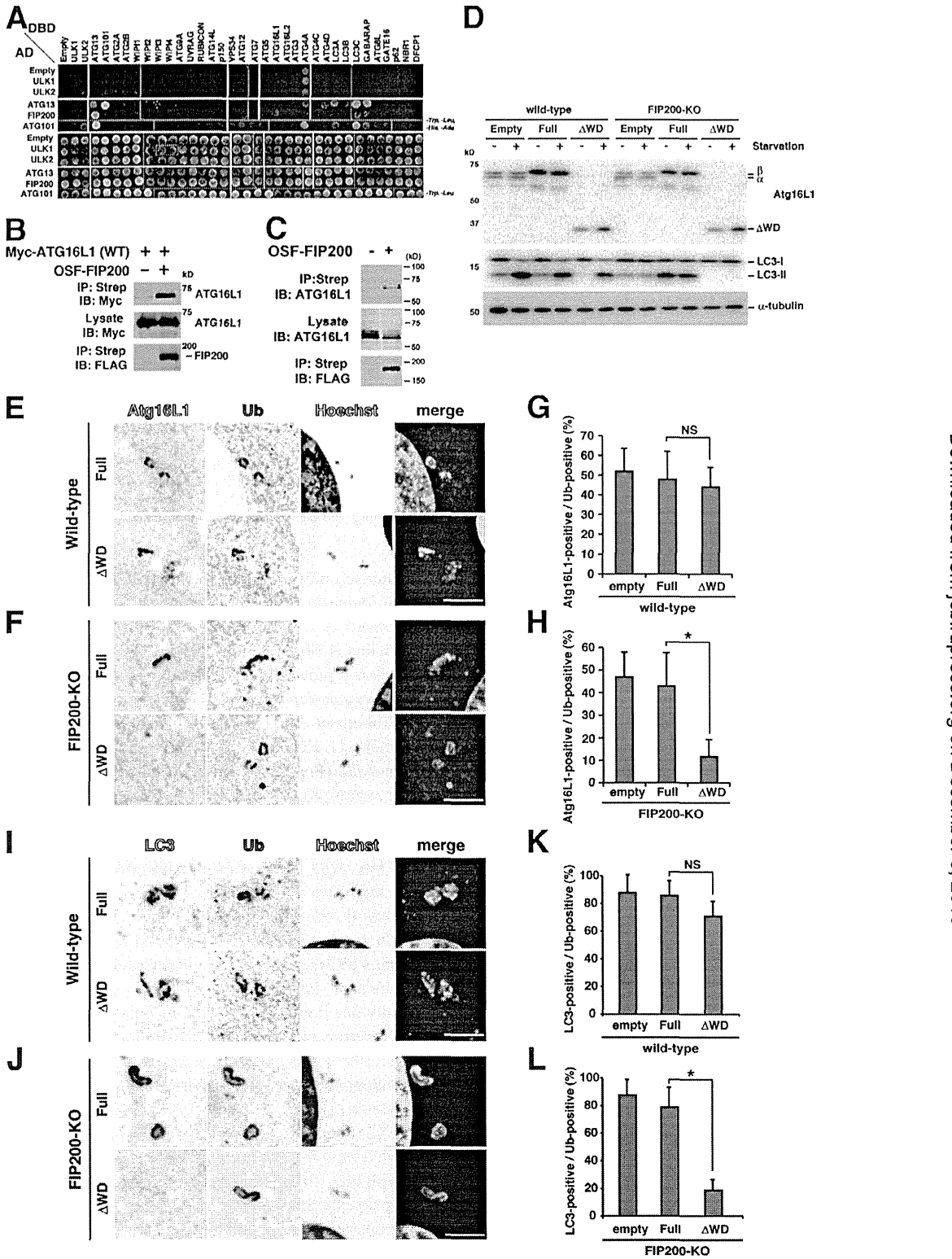

Figure 4. **The WD β-propellers of Atg16L1 recruit LC3 in the absence of FIP200.** (A) Yeast two-hybrid interactions of the ULK1 complexes with other human Atg proteins. ULK1, ULK2, Atg13, FIP200, and Atg101-AD fusions (rows 2–6) or control AD constructs (row 1, Empty) were coexpressed with control DBD constructs (column 1, Empty) or Atg protein–DBD fusions (columns 2–35) and tested for positive yeast two-hybrid interactions (top) or cotransformation (control, bottom). White lines divide images derived from the same plate, and red lines divide images from different plates. Atg16L1 positively interacted with FIP200 in this assay. (B) FIP200 binds to exogenously expressed Atg16L1. Myc-Atg16L1 coprecipitations with an empty vector control (lane 1) or One-STrEP-FLAG

Published October 7, 2013

GST alone. In contrast, the ΔWD mutant did not bind to GST-Ub (Fig. 3 C). Next, we prepared recombinant trigger factor–FLAG-tagged WD β-propellers of Atg16L1 using bacteria (Fig. S3 B). A GST pull-down experiment was performed with these recombinant proteins. The WD β-propellers bound to GST-Ub more efficiently than to GST alone (Fig. 3 D). From these results, we concluded that there is a direct interaction between the WD β-propellers of Atg16L1 and Ub.

Atg16L1 is recruited by binding to Ub and FIP200

Although Atg16L1 could bind to Ub, deleting the WD β-propellers only minimally affected Atg16L1 recruitment to invading *Salmonella* (Fujita et al., 2009), suggesting that binding to Ub is not sufficient for Atg16L1 recruitment and additional interacting partner(s) functions in the recruitment. Thus, we searched for the Atg16L1 complex–interacting proteins using mass spectrometry. We found that ULK1 and FIP200 coimmunoprecipitated with the Atg16L1 complex, which consists of Atg16L1, Atg12, and Atg5 (Table S1). Because ULK1 forms a large protein complex including ULK1/2, Atg13, FIP200, and Atg101 (Mizushima, 2010), we performed a direct yeast two-hybrid assay with these proteins and found that Atg16L1 directly interacts with FIP200 (Fig. 4 A). The interaction was also confirmed by immunoprecipitation experiments (Fig. 4, B and C). Thus, we found that Atg16L1 binds to FIP200 in addition to Ub.

Next, to test the roles of these interactions in autophagy, we generated Atg16L1-replaced wild-type and FIP200-KO cells (Fig. 4 D). We previously reported that stably expressing an exogenous Atg16L1 construct can replace the endogenous Atg16L1 protein with the exogenous one (Fujita et al., 2009; see legend of Fig. 4 for more details). In sharp contrast to wild-type cells, in FIP200-KO cells the recruitment of Atg16L1 to Ub-positive *Salmonella* and beads depended on the WD β-propellers (Fig. 4, E and H; and unpublished data). Next, we examined the effect of deleting the WD β-propellers on LC3 recruitment to Ub-positive *Salmonella* or beads because the Atg16L1 complex functions as an E3-like factor in the LC3 system (Fujita et al., 2008b). In wild-type cells, LC3 recruitment was not remarkably affected by deleting the WD β-propellers as was previously reported (Fig. 4, I and K; Fujita et al., 2009). On the contrary, deleting the WD β-propellers significantly decreased the localization of LC3 to Ub-positive *Salmonella* and beads in FIP200-KO cells (Fig. 4, J and L; and unpublished data). We also confirmed that LC3 lipidation was totally dependent on the WD β-propellers of Atg16L1 (Fig. 4 D). These results show that the localization of the Atg16L1 complex to Ub-positive *Salmonella* or beads involves interactions with both Ub via the WD β-propellers and FIP200, resulting in PE conjugation of LC3. Because the ULK1–FIP200 complex recruitment also depends on ubiquitination (Fig. 2 C), Atg16L1 must recognize Ub on the target through two mechanisms, one of which is direct recognition and the other is indirect.

To address the impact of the WDR-mediated mechanisms on the order of the Atg16L1 and ULK1–FIP200 complex recruitment, we quantified the localization of ULK1 and Atg16L1 in Ub-positive *Salmonella* in Atg16L1-reconstituted cells. The deletion of WDR did not affect the percentage of Atg16L1-positive in ULK1-GFP–positive population (Fig. S4 B). In sharp contrast to this, the deletion of WDR significantly decreased the percentage of Atg16L1-positive in ULK1-GFP–negative population (Fig. S4 C). These results suggest that the FIP200 is recruited to the Ub-positive *Salmonella* before Atg16L1 in the absence of WDR-mediated mechanisms.

Atg16L1 recognizes the target via three pathways

We further explored the interaction between Atg16L1 and FIP200. Using a yeast two-hybrid analysis, we found that Atg16L1 bound to both the FIP200-N (1–840) and FIP200-C (1276–1591) fragments (Fig. 5 A), whereas the Atg16L1 ΔWD mutant (1–246) bound only to FIP200-C (Fig. 5, B and E). We decided to focus on the interaction between Atg16L1 and the FIP200-C fragment in order to determine why ΔWD can fulfill autophagic functions in the presence of FIP200. In a yeast two-hybrid analysis, the FIP200-C fragment bound to the Atg16L1 (1–246) fragment but not to the Atg16L1 (1–230) fragment, suggesting the importance of residues 230–246 for this interaction (Fig. 5 B). Thus, we performed alanine scanning in this region, and found that residues 239–246 were important for this interaction (Fig. 5, C and D). We confirmed the impact of 239–242A mutations within Atg16L1 on its ability to interact with the FIP200-C fragment in an immunoprecipitation experiment (Fig. 5 F). Thus, we obtained an Atg16L1 mutant that lacks affinity for FIP200.

We then generated a series of cells reconstituted with various Atg16L1 mutants in which Atg16L1Δ/Δ MEFs stably express the above-mentioned Atg16L1 constructs (Fig. 6 A; and Fig. S5 A). The Atg16L1-reconstituted cells were challenged with *Salmonella* or transfected with beads, and the percentages of LC3- or Atg16L1-positive per Ub-positive were counted. The

(OSF)-FIP200 (lane 2). (C) FIP200 binds endogenous Atg16L1. Atg16L1 coprecipitations with an empty vector control (lane 1) or OSF-FIP200 (lane 2). (D) Wild-type or FIP200-KO MEFs stably expressing the empty vector, full-length Atg16L1, or ΔWD mutant were incubated in growth medium (−) or Earle's balanced salt solution (EBSS) (+) for 1 h and examined by Western blotting using the indicated antibodies. We previously reported that stable expression of an exogenous Atg16L1 construct can be used to replace the endogenous Atg16L1 protein with an exogenous Atg16L1 protein (Fujita et al., 2009) because free Atg16L1 molecules not complexed with the Atg12–Atg5 conjugate are preferentially degraded by the ubiquitin–proteasome system. In control cells (Empty), two Atg16L1 splicing variants, the α- and β-forms, were detected. In full-length β-form–replaced cells (Full), the α-form was not detected, whereas in ΔWD-replaced cells (ΔWD) both the α- and β-forms were minimally detected. Thus, we successfully obtained cells that express only endogenous levels of the full-length or ΔWD mutant. (E–L) Atg16L1-replaced wild-type or FIP200-KO MEFs were infected with *Salmonella* (MOI = 10) for 1 h and subjected to immunocytochemistry for Atg16L1 and Ub (E and F) or LC3 and Ub (I and J). The percentages of Atg16L1-positive (G and H) or LC3-positive per Ub-positive bacteria were enumerated (K and L). At least 50 *Salmonella* were counted. The average ± SD is shown for three independent experiments. Statistical analysis was performed by Student's *t* test. *, $P < 0.05$; NS, not significant. Bar, 5 µm.

Published October 7, 2013

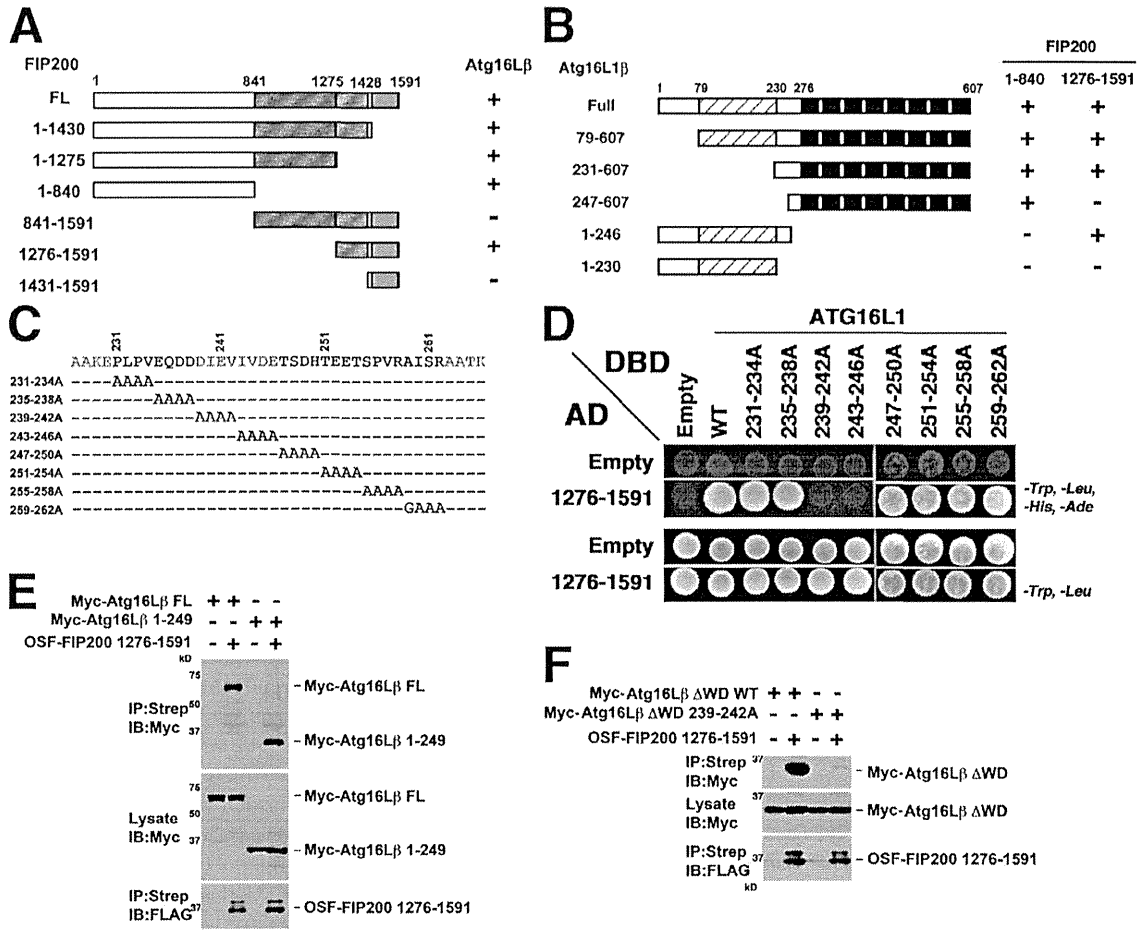

Figure 5. **Atg16L1-FIP200 interacting domains.** (A) Mapping of the Atg16L1-binding site on FIP200. Yeast two-hybrid mapping experiments showing that Atg16L1 binds to both the N-terminal and C-terminal coiled-coil regions of FIP200. (B) Mapping of the FIP200-binding site within Atg16L1. Yeast two-hybrid mapping experiments showing that the 1–840 fragment of FIP200 binds to the C-terminal 247–607 region, while the 1276–1591 fragment of FIP200 binds to the N-terminal 1–264 region of Atg16L1. (C and D) Additional yeast two-hybrid mapping experiments showing that the binding site of the FIP200 1276–1591 fragment maps to residues 239–246 of Atg16L1. White lines divide images derived from the same plate, and red lines divide images from different plates. (E) The N-terminal 1–249 fragment of Atg16L1 is sufficient to interact with FIP200. Full-length (lanes 1 and 2) or the N-terminal 1–249 fragments (lanes 3 and 4) of Myc-Atg16L1 coprecipitations with empty vector controls (lanes 1 and 3) or OSF-FIP200 1276–1591 (lanes 2 and 4). (F) Co-precipitation experiments confirming that OSF-FIP200 1276–1591 coprecipitates with wild-type (WT) Myc-Atg16L1 (1–249) fragments, but not with analogous fragments containing a mutant FIP200-binding site (Myc-Atg16L1 ΔWD 239–242A).

localization of LC3 or Atg16L1 to invading bacteria and transfected beads was slightly affected by the ΔWD + 239–242A mutation, but not significantly abolished (Fig. 6, B–E; and Fig. S5, C–F). This suggests that, besides interactions with FIP200 and Ub, another mechanism functions to localize the Atg16L1 complex in selective autophagy. We previously reported that residues 193–230 in Atg16L1 are essential for the inhibitory effects of excess Atg16L1 on autophagy (Itoh et al., 2008). Thus, we further explored this region and found that substituting residues W194 and M195 with alanine (194–195A) synergistically affected the function of Atg16L1 in both canonical and selective autophagy (Fig. 6 and Fig. S5). Although the W194–M195 mutations alone slightly affected autophagic activity, a combination of 239–242A, 194–195A, and the ΔWD mutation synergistically reduced the recruitment of LC3 and Atg16L1 to the ubiquitinated substrate. Thus, we propose that the Atg16L1 complex localizes and directs LC3 to ubiquitinated substrates through these three independent mechanisms.

Intriguingly, in contrast to selective autophagy, starvation-induced nonselective autophagy requires only Ub and FIP200 binding of Atg16L1 (Fig. 6 F and Fig. S5). Full-length 239–242A minimally affected both PE conjugation and LC3 puncta formation in starvation-induced autophagy (Fig. 6 F; and Fig. S5, A and G). Furthermore, deleting the WD β-propellers in Atg16L1 minimally affected autophagosome formation and p62 degradation (Fig. 6 F; and Fig. S5, B and G), as we previously reported (Fujita et al., 2009). In sharp contrast to these mutants, a combination of the ΔWD and 239–242A mutations almost completely reduced LC3 puncta formation under starvation conditions (Fig. 6 F). We also confirmed that the ΔWD + 239–242A mutation significantly reduced the number of Atg16L1 puncta (Fig. S5 H). Therefore, FIP200 binding and the WD β-propellers of Atg16L1

Published October 7, 2013

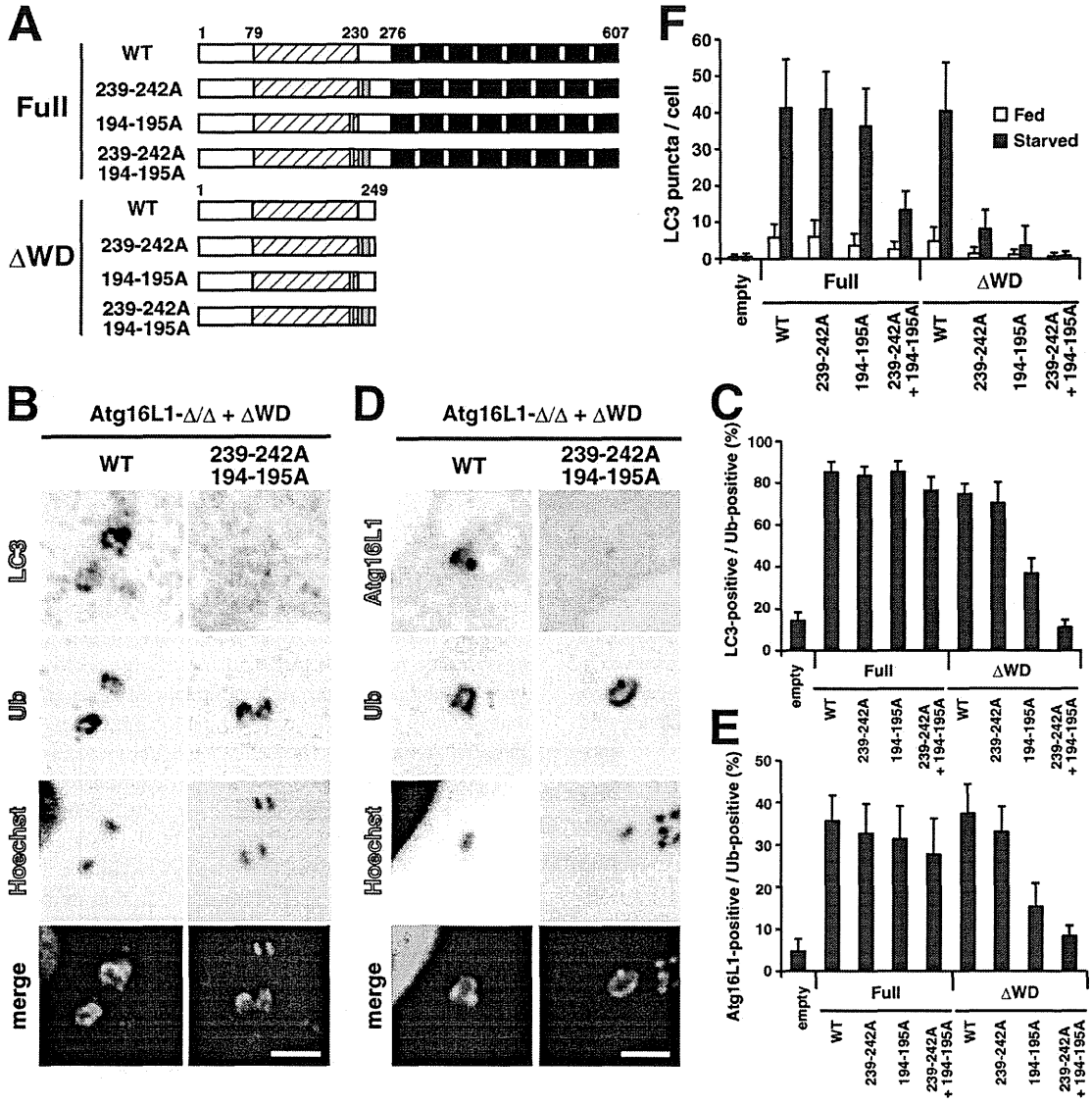

Figure 6. **Effects of Atg16L1 mutations on autophagy against *Salmonella*.** (A) Schematic diagram of Atg16L1 and various mutants. The magenta box indicates 239–242A and the cyan box indicates 194–195A. (B–E) Atg16L1-Δ/Δ MEFs stably expressing the indicated constructs were infected with *Salmonella* (MOI = 10) for 1 h and then analyzed by immunocytochemistry for LC3 (B) or Atg16L1 (D). Bar, 5 µm. The percentage of LC3- or Atg16L1-positive *Salmonella* per Ub-positive *Salmonella* was enumerated by fluorescence microscopy (C and E). At least 50 bacteria were counted. The average ± SD is shown for three independent experiments. (F) Atg16L1-Δ/Δ MEFs stably expressing the indicated constructs were cultured in growth medium (Fed) or EBSS (Starved) for 1 h and then subjected to immunocytochemistry using an anti-LC3 antibody. The number of LC3 puncta in each cell was counted for more than 50 cells. The average ± SD is shown for three independent experiments.

are sufficient to localize the Atg16L1 complex under starvation conditions, indicating that there are different mechanisms in selective and nonselective autophagy.

Discussion

In this paper, we revealed that ubiquitination plays an important role in the autophagic response to invading pathogens, notable *Salmonella*. First, we have shown that the endosomal membrane surrounding *Salmonella* and latex beads is ubiquitinated. Second, ubiquitination is necessary for recruiting three pivotal components of the autophagic machinery, notably the Atg16L1 complex, the ULK1 complex, and Atg9L1. Third, Atg16L1 directly binds to Ub and FIP200. These interactions are redundant in both starvation-induced and autophagy against *Salmonella*/transfected bead. Thus, we have provided molecular evidence of the ubiquitinated target and determined how ubiquitination recruits the autophagic machinery (Fig. 7).

Our model is significantly different from the current prevailing model in which bacteria that have escaped into the cytosol are ubiquitinated and targeted by autophagy (Thurston et al., 2009; Yoshikawa et al., 2009; Zheng et al., 2009; Wild et al., 2011). Consistent with our model, electron microscopic analysis showed that a significant fraction of bacteria within cells is

Published October 7, 2013

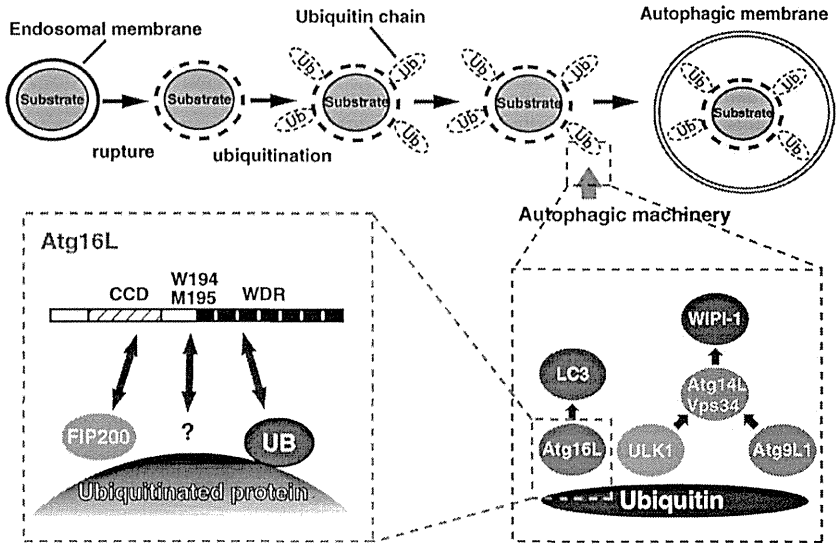

Figure 7. **A possible mechanism of Ub-mediated autophagic sequestration of invading bacteria and transfection reagent–coated latex beads.** After internalization and endosomal rupture, Ub is conjugated to host cellular proteins in endosomes that contain *Salmonella* or transfection reagent–coated latex beads (top). Ub would be recognized by three pivotal components of the autophagic machinery, notably the Atg16L1 complex, the ULK1 complex, and Atg9L1 (bottom right). Atg16L1 localizes to the ubiquitinated target through three mechanisms, the interaction of coiled-coil domain (CCD) with FIP200, the interaction of WD repeats (WDR) with Ub, and the 194–195 region-mediated mechanism (bottom left).

contained within multilamellar compartments (Zheng et al., 2009; Kageyama et al., 2011). Our model is also consistent with these two recent papers that diacylglycerol (DAG) is involved in selective autophagy (Shahnazari et al., 2010), as the localization of DAG surrounding *Salmonella* indicates the existence of a membrane, and galectin8 targets damaged endosomes to autophagy via an NDP52-mediated mechanism (Thurston et al., 2012). It is still unclear how host endosomal proteins are ubiquitinated. Upon membrane rupture, the lumenal side of endosomal proteins is exposed to the cytosol, which may lead to their ubiquitination. Alternatively, a drastic change in the endosomal ion concentrations may trigger ubiquitination. In any case, host cells likely have a simple and common mechanism that targets invading pathogens for selective autophagy, despite differences in the invading bacterial species. If bacterial proteins are directly ubiquitinated, diverse E3 ligases are required to recognize and target diverse bacterial species and it will be important to identify the E3 ligase(s) that function in selective autophagy. Furthermore, we do not exclude the possibility that bacterial proteins are ubiquitinated; however, our data indicate that neither bacterial escape from endosomes nor the ubiquitination of bacteria are essential for selective autophagy. It was previously shown that membrane remnants resulting from the endosomal escape of *Shigella flexneri* in infected cells colocalized with polyubiquitinated proteins and were targeted for autophagic degradation (Dupont et al., 2009). These membrane remnants were likely targeted by a similar mechanism that is used to degrade other invading bacteria. All bacteria that enter the cytosol have to cross a membrane, which possibly involves membrane rupture. Therefore, the recognition of Ub-positive damaged membranes might be a general mechanism that can respond to different types of invading bacteria.

Ub has been generally proposed to play a role in selective autophagy. Very recently, it has been reported that LRSAM1 functions as the E3 ligase responsible for Ub-mediated anti-*Salmonella* autophagy (Huett et al., 2012). In this study, we showed that blocking ubiquitination by an E1-specific inhibitor leads to a defect in selective autophagy using latex beads and a galectin3 marker system. We further substantiated these findings by discovering that Atg16L1 directly binds Ub. In the absence of ubiquitination, the recruitment of other pivotal Atg units, notably the ULK1 complex and Atg9L1, was disrupted (Fig. 2 C). It has been proposed that adaptor molecules, such as p62, NDP52, and optineurin, bridge ubiquitinated substrates and autophagosomal membranes through LC3 (Thurston et al., 2009; Yoshikawa et al., 2009; Zheng et al., 2009; Wild et al., 2011). This model predicts that adaptors recruit the autophagic machinery as an LC3-positive structure. In this study, we systematically explored the hierarchy of Atg proteins in selective autophagy and found that three Atg functional units, the ULK1 complex, Atg9L1, and the Atg16L1 complex localized to ubiquitinated substrates independently of other Atg proteins (Fig. 2, D and E; Fig. S1; and Fig. 7). Furthermore, we showed that LC3 localized to these substrates after the appearance of these three units. Our data indicate that LC3 is dispensable for the initial stage of selective autophagy. However, we note that it is possible that the adaptor–LC3 interaction might function in other aspects, such as a zipper between ubiquitinated substrates and autophagosomal membranes to facilitate efficient enwrapping.

Although we used an E1 inhibitor to block ubiquitination, the drug blocks all of the ubiquitination reactions in the cells nonspecifically, which might affect Atg protein recruitment indirectly. LRSAM1 contributes the ubiquitination to invading bacteria. However, invading bacteria are still ubiquitinated even in LRSAM1-deficient cells (Huett et al., 2012), indicating that other E3 enzyme(s) besides LRSAM1 is also involved in the ubiquitination accompanying bacteria invasion. To test the contribution of ubiquitination to selective autophagy more directly, a set of E3 enzymes should be identified in the future studies.

Our data and the previous report indicate that at least K48-, K63-, and linear-linked Ub chains localize to the invading *Salmonella* (Fig. S2 A; van Wijk et al., 2012). And in vitro *Salmonella* ubiquitination reaction by LRSAM1 predominantly induces K6- and K27-linked Ub chains (Huett et al., 2012).

Published October 7, 2013

These evidences indicate that different Ub-linkages could be part of the Ub-coat on the invading *Salmonella*. Further, we showed that autophagic machinery targeting did not depend solely on K63- or linear-Ub linkages (Fig. S2, B and C). These results suggest that autophagic machinery could target different Ub linkages, or other linkages besides K63 and linear might be specifically favored by autophagic machinery.

Atg16L1 directly interacts with ubiquitin and FIP200 through the WD β-propellers and residues 239–242, respectively (Figs. 3–5). The WD β-propellers of Atg16L1 are required to localize the Atg16L1 complex and LC3 to ubiquitinated substrates in the absence of FIP200 (Fig. 4, E–L). This result explains our previous observation that LC3 localized to a single membrane in *Salmonella*-infected FIP200-KO cells (Kageyama et al., 2011). Because the WD β-propellers have an affinity for Ub (Fig. 3) and host cellular proteins are ubiquitinated upon bacterial invasion (Fig. 1 and Fig. S1), PE conjugation of LC3 could occur in Ub-positive endosomal membranes in FIP200-KO cells. We do not have a clear answer as to why Atg16L1 has dual (or triple) recruiting mechanisms. It is noteworthy that Atg16 in simple eukaryote-like budding yeast lacks the WD β-propellers. One interesting possibility is that higher eukaryotes such as mammals have evolved to use autophagy to clear invading pathogens, and to secure such a complex process Atg16L1 may be involved in a back-up system. Interestingly, the WD β-propellers also seem to be involved in starvation-induced autophagy. p62-positive foci are observed at the autophagosome formation site (Itakura and Mizushima, 2010). We also observed Ub-positive signals at the starvation-induced autophagosome formation site (unpublished data). Thus, mammals may be evolved to use the Ub-binding capacity of Atg16L1 in starvation-induced autophagy.

A combination of Atg16L1 239–242A and ΔWD mutations severely impaired starvation-induced autophagy (Fig. S5), while selective autophagy against invading pathogens still occurred (Fig. 6; and Fig. S5, C–F). This indicates that interactions between Atg16L1 and FIP200 or Ub are not sufficient to localize the Atg16L1 complex in selective autophagy. We identified other important amino acids, 194–195 in Atg16L1 (Fig. 6 and Fig. S5). Because the ΔWD, 239–242A, and 194–195A mutations synergistically reduced the recruitment of Atg16L1 to the substrate (Fig. 6 and Fig. S5), we propose that all of these regions help localize the Atg16L1 complex to the ubiquitinated substrate (Fig. 7). Because residues 194–195 of Atg16L1 do not appear to be involved in FIP200 binding, Atg16L1 dimerization, or interactions with other Atg proteins (unpublished data), the region could interact with an unidentified factor. Interestingly, the Atg16L1 ΔWD construct contains the 194–195 region, although expression of the ΔWD mutant severely blocked LC3 recruitment in FIP200-KO cells (Fig. 4, J and L). The absence of a double membrane in these cells may lead to loss of the interaction partner for the 194–195 region, although we do not know the target(s) of this region.

In this study, we have uncovered the mechanisms by which selective autophagy responds to invading pathogens and shown that ubiquitinated substrates are recognized by the Atg16L1 complex independently of an LC3-mediated mechanism. These discoveries are similar to another Ub-mediated endosomal process, the multi-vesicular body pathway. Cargo proteins are ubiquitinated and the molecular machinery involved in this pathway, called ESCRT, is recruited by directly binding to Ub (Katzmann et al., 2001). Furthermore, our model may be applicable to Parkin-mediated autophagy against mitochondria, in which mitochondria are also decorated with Ub (Youle and Narendra, 2011). Thus, we provide a novel role for Ub among its many diverse functions. Our findings will open up new avenues in the study of autophagy.

Materials and methods

Reagents and antibodies

Cell culture reagents were purchased from Invitrogen. The following antibodies were used: anti–mouse Atg16L1 (Mizushima et al., 2003), anti-p62 (MBL), anti-LC3 (MBL), anti-transferrin receptor (Invitrogen), anti-poly Ub (clone FK2; BIOMOL), anti-K48 linked Ub (clone Apu2; EMD Millipore), anti-K63 linked Ub (clone Apu3; EMD Millipore) anti-galectin3 (Santa Cruz Biotechnology, Inc.), anti-Lamp1 (Santa Cruz Biotechnology, Inc.), anti-FLAG (clone M2; Sigma-Aldrich), anti-GFP (Roche), anti-Myc (clone 9E10), and anti–α-tubulin (clone B5-1-2; Sigma-Aldrich). All other reagents were purchased from Sigma-Aldrich.

DNA engineering and recombinant retroviruses

The pMRX-IRES-puro and pMRX-IRES-blast vectors were gifts from S. Yamaoka (Tokyo Medical and Dental University, Tokyo, Japan; Saitoh et al., 2003). To generate recombinant retroviruses, cDNAs corresponding to mStrawberry (mStr)-tagged galectin3, mStr-Ub, GFP-Ub, and GFP-p62 were subcloned into the pMRX-IRES-puro vector. Various human Atg16L1β (isoform-1) mutants were cloned into the pMRX vector, including full-length (1–607), ΔWD repeat domain (1–249), and the Crohn's disease–associated mutant (T300A; Fujita et al., 2009). In addition, pMRX constructs were generated to encode various GFP-tagged Atg proteins, including LC3 (N terminus), Atg5 (N terminus), WIPI1 (N terminus), Atg14L (N terminus), Atg9L1 (C terminus), and ULK1 (C terminus; Kageyama et al., 2011), as previously reported. Recombinant retroviruses were prepared as previously described (Saitoh et al., 2003). To prepare recombinant proteins, cDNA corresponding to Ub was subcloned into the pGEX6P-1 vector, and cDNA corresponding to FLAG-tagged wild-type or the Crohn's disease–associated mutant of the WD β-propellers of Atg16L1 was subcloned into the pCold-TF vector (Takara Bio Inc.).

Cell culture and retroviral infections

Plat-E cells were provided by T. Kitamura (The University of Tokyo, Tokyo, Japan; Morita et al., 2000). HeLa cells, HEK293T cells, NIH3T3 cells, wild-type MEFs, and autophagy-deficient MEFs (Atg5-KO, Atg14L-KO, Atg9L1-KO, Atg16L1-Δ/Δ, and FIP200-KO) were grown in DMEM supplemented with 10% fetal bovine serum, 2 mM L-glutamine, 5 U/ml penicillin, and 50 U/ml streptomycin in a 5% CO_2 incubator at 37°C (Kuma et al., 2004; Fujita et al., 2008a; Saitoh et al., 2008, 2009; Hara and Mizushima, 2009; Matsunaga et al., 2009; Nishimura et al., 2013). Stable transformants were selected in growth medium with 1 μg/ml puromycin or 5 μg/ml blasticidin (Invivogen).

Western blotting

Samples were subjected to SDS-PAGE, and transferred to polyvinylidene fluoride membranes. The membranes were blocked with TBST (TBS and 0.1% Tween 20) containing 1% skim milk and were then incubated overnight at 4°C with primary antibodies 1,000–3,000× diluted in the blocking solution. Membranes were washed three times with TBST, incubated for 1 h at room temperature with 10,000× dilutions of HRP-conjugated secondary antibodies (GE Healthcare) in the blocking solution, and washed five times with TBST. Immunoreactive bands were then detected using ECL plus (GE Healthcare) and a chemiluminescence detector (LAS-3000, Fujifilm; Kimura et al., 2009).

Bacterial infections and bead transfections

Salmonella enterica serovar Typhimurium (SR-11 x3181) was provided by the Research Institute of Microbial Disease, Osaka University (Osaka, Japan). Bacteria were grown overnight at 37°C, and then sub-cultured at

Published October 7, 2013

1:33 for 3 h in LB without antibiotics. The bacterial inocula were prepared by pelleting at 10,000 *g* for 2 min, and were then added to host cells at a multiplicity of infection (MOI) of 10–100 at 37°C with 5% CO_2 (Kageyama et al., 2011). Bead transfections were performed as previously reported (Kobayashi et al., 2010). Transfection reagent-coated beads were prepared by mixing the beads (NH_2-, 17145-5; PolySciences, Inc.) with Effectene transfection reagent (301425; QIAGEN), according to the manufacturer's instructions except that bead suspension was used instead of DNA solution. The resulting bead mixture (~100 µl) was further mixed with 1 ml of growth medium, and added to cells by replacing the medium. After incubation with the bead mixture for 1 h at 37°C in a CO_2 incubator, the cells were washed twice with fresh growth medium to remove unattached beads, and further incubated for the time indicated in each experiment.

Immunofluorescence and microscopy

Cells were cultured on coverslips, fixed with 3% PFA in PBS for 10 min, and permeabilized with 50 µg/ ml digitonin in PBS for 5 min. Cells were then treated with 50 mM NH_4Cl^-/PBS for 10 min at room temperature and blocked with PBS containing 3% BSA for 15 min. Primary antibodies were diluted 1:500 or 1:1,000, and Alexa Fluor–conjugated secondary antibodies (Invitrogen) were diluted 1:1,000 in PBS containing 3% BSA. Coverslips were incubated with primary antibodies for 60 min, washed six times with PBS, and incubated with secondary antibodies for 60 min. Samples were mounted using Slow Fade Gold and observed with an laser confocal microscope (FV1000; Olympus). The microscope images were taken using the FV1000 confocal laser-scanning microscope system equipped with a 100x/NA 1.40 oil immersion objective lens. Fluorochromes associated with the secondary antibodies were Alexa Fluor 405, 488, 568, or 594. Image acquisition software used was Fluoview (Olympus). The images were adjusted using Photoshop CS4 software (Adobe). For live-cell imaging, cells were grown in DMEM D6434 (Sigma-Aldrich) supplemented with 10% FBS with antibiotics on a glass-bottom dish (D310300; Matsunami Glass) and transfected with Effectene-coated latex beads for 30 min as previously described (Kobayashi et al., 2010). After beads transfection, the glass-bottom dish was mounted onto the microscope stage, which was equipped with a humidified environment chamber (MI-IBC; Olympus) that maintained the dish at 37°C with 5% CO_2. Images were acquired using an inverted microscope (model IX81; Olympus) equipped with a 60x/1.40 NA oil immersion objective (Olympus), a xenon lamp, a cooled charge-coupled device camera (CoolSNAP HQ; Roper Scientific), and a ZDC system under the control of MetaMorph v7.6.5.0 (Molecular Devices, MDS Analytical Technologies).

GST pull-down assay

GST and GST-Ub were purified from *Escherichia coli* lysates over glutathione Sepharose 4B (GE Healthcare) and dialyzed in PBS. 30 µg of each GST protein immobilized on 30 µl of glutathione Sepharose 4B was used per binding reaction. Mammalian cell lysates or bacterial cell lysates were used as the input proteins. HEK293T cells were transiently transfected with plasmids encoding the indicated Atg16L1 constructs, homogenized in PBS containing protease inhibitors (complete protease inhibitor cocktail; Roche), and then cleared by centrifugation and filtration (0.22 µm). Alternatively, *E. coli* BL-21 (DE3) cells expressing trigger factor–fused FLAG-WD β-propellers of Atg16L1 were sonicated in PBS containing 0.01% Triton X-100 and protease inhibitors and cleared by centrifugation and filtration (0.22 µm). Immobilized beads and cell lysates were incubated in a total volume of 500 µl PBS containing 0.1 mg/ml BSA and 0.01% Triton X-100 with gentle agitation for 1 h at 25°C. The beads were washed three times with ice-cold PBS and the bound complexes were eluted with 50 mM reduced glutathione in PBS and then subjected to SDS-PAGE and Western blot analyses.

Fractionation of bead–autophagosomes

Bead–autophagosomes were isolated using a modification of the method described by Desjardins et al. (1994). HeLa cells were transfected with Effectene-coated beads and incubated for 3 h. The cells were harvested with a silicone rubber scraper and homogenized in buffer (20 mM Hepes-KOH, pH 7.4, 80 mM sucrose, 220 mM mannitol, 10 mM *N*-ethylmaleimide, 1 mM PMSF, and a protease inhibitor cocktail [Roche]) by repeatedly passing (~15 times) through a 1-ml syringe with a 25-gauge needle. The homogenate was centrifuged at 1,000 *g* for 10 min to remove the cytosol and microsomes. The bead–autophagosomes were isolated by flotation on a discontinuous gradient composed of 1 ml each of increasing concentrations of sucrose solutions (60, 40, 35, 30, 25, 20, 15, 10, and 5%; all sucrose solutions were wt/wt in 3 mM imidazole, pH 7.4). The resulting pellet was resuspended in a 25% sucrose solution and loaded on top of a 30% sucrose solution. The samples were centrifuged in a swinging bucket rotor (SW41Ti; Beckman Coulter) for 1 h at 100,000 *g* at 4°C. The bead-autophagosome–containing fraction was collected from the interface of the 10 and 15% sucrose solution. The bead–autophagosomes were resuspended in 2 ml of ice-cold PBS and pelleted by centrifuging for 10 min at 20,000 *g* at 4°C.

Yeast two-hybrid assays

Yeast two-hybrid assays were performed using the Matchmaker GAL4 Yeast Two Hybrid 3 system (Takara Bio Inc.) as previously reported (Langelier et al., 2006). *Saccharomyces cerevisiae* AH-109 was cotransformed with the cloning vectors, pGADT7 or pGBKT7, containing the inserts of interest. The transformed yeast cells were incubated on yeast nitrogen base and glucose with minus Leu, minus Trp selection for 3 d at 30°C. 10–100 colonies were resuspended in a liquid culture of Sabourand dextrose broth (minus Leu, minus Trp), and incubated on Sabourand dextrose broth (minus Leu, minus Trp, minus Ade, minus His) plates for 3 d.

Identification of co-purifying proteins by mass spectrometry

HEK293T cells were seeded (3 × 10^6 cells/55-cm^2 dish) and cotransfected with 3 µg each of plasmids encoding members of the Atg16L1 complex (Atg12, Atg5, and Atg16L1) using polyethylenimine (25,000 kD; Polysciences, Inc.) as previously described (Durocher et al., 2002). The cells were harvested 48 h after transfection by incubating in 300 µl lysis buffer (50 mM Tris, pH 7.4, and 150 mM NaCl) supplemented with proteinase inhibitor cocktail (Roche) and 1% Triton X-100. Lysates were clarified by centrifugation (18,000 *g*, 10 min, 4°C) and incubated with Strep-Tactin Sepharose (30 µl slurry, 2 h, 4°C; IBA GmbH). The matrix was washed four times in wash buffer (20 mM Tris, pH 7.4, and 150 mM NaCl) supplemented with 0.1% Triton X-100, and the purified Atg16L1 complexes were eluted with 2.5 mM desthiobiotin. The co-purified proteins were identified by mass spectrometry. Briefly, the co-purified proteins were identified after SDS-PAGE and band excision. The proteins were digested with trypsin and identified by separating the peptide mixtures using nano-flow liquid chromatography with online tandem mass spectrometry (LC-MS/MS). Tandem mass spectra were acquired automatically and then searched against a nonredundant human database from the NCBI database with the Mascot Server (Matrix Science).

Statistics

All values in the figures are shown with standard deviation. Statistical analyses were performed using a two-tailed unpaired *t* test. P values <0.05 were considered statistically significant.

Online supplemental materials

Fig. S1 shows the result of hierarchal analysis of Atg proteins in bead-transfected cells. Fig. S2 shows localization of K48- and K63-linked Ub chains to the invading *Salmonella* or transfected beads, and loss of function effect of K63- or linear-linked Ub chains on selective autophagy. Fig. S3 shows the purity of the recombinant proteins for the GST pull-down assay. Fig. S4 shows the effect of deletion of WDR in Atg16L1 on the order of the Atg16L1 and ULK1-FIP200 complex recruitment to Ub-positive *Salmonella*. Fig. S5 shows the effect of Atg16L1 mutations on canonical and selective autophagy against transfected beads. Videos show dynamics of LC3 and galectin3 (Video 1), Ub and galectin3 (Video 2), LC3 and Ub (Video 3), Atg5 and Ub (Video 4), WIPI-1 and Ub (Video 5), Atg14L and Ub (Video 6), or ULK1 and Ub (Video 7) in autophagy against transfected beads. Table S1 provides a list of FIP200 peptides detected by affinity purification with the Atg16L1 complex and mass spectrometry analysis. Online supplemental material is available at http://www.jcb.org/cgi/content/full/jcb.201304188/DC1.

The authors thank R.Y. Tsien for the gift of mStrawberry cDNA; S. Yamaoka for providing pMRX-IRES-puro and pMRX-IRES-bsr; T. Kitamura for providing the Plat-E cells; N. Mizushima for the anti-Atg16L1 antibody; K. Okamoto for helpful discussions; S. Cox for English editing of the manuscript; and R. Tsukahara and H. Akai for technical assistance. LC-MS/MS analysis was performed in the DNA-chip Development Center for Infectious Diseases (RIMD, Osaka University).

This work was supported in part by the Ministry of Education, Culture, Sports, Science and Technology (MEXT; to N. Fujita, S. Kobayashi, T. Haraguchi, T. Noda, and T. Yoshimori); and the Takeda Science Foundation (to T. Yoshimori and T. Noda).

Submitted: 29 April 2013
Accepted: 4 September 2013

Published October 7, 2013

References

Birmingham, C.L., and J.H. Brumell. 2006. Autophagy recognizes intracellular *Salmonella enterica* serovar Typhimurium in damaged vacuoles. *Autophagy*. 2:156–158.

Desjardins, M., L.A. Huber, R.G. Parton, and G. Griffiths. 1994. Biogenesis of phagolysosomes proceeds through a sequential series of interactions with the endocytic apparatus. *J. Cell Biol.* 124:677–688. http://dx.doi.org/10.1083/jcb.124.5.677

Dupont, N., S. Lacas-Gervais, J. Bertout, I. Paz, B. Freche, G.T. Van Nhieu, F.G. van der Goot, P.J. Sansonetti, and F. Lafont. 2009. *Shigella* phagocytic vacuolar membrane remnants participate in the cellular response to pathogen invasion and are regulated by autophagy. *Cell Host Microbe*. 6:137–149. http://dx.doi.org/10.1016/j.chom.2009.07.005

Durocher, Y., S. Perret, and A. Kamen. 2002. High-level and high-throughput recombinant protein production by transient transfection of suspension-growing human 293-EBNA1 cells. *Nucleic Acids Res.* 30:E9. http://dx.doi.org/10.1093/nar/30.2.e9

Fujita, N., M. Hayashi-Nishino, H. Fukumoto, H. Omori, A. Yamamoto, T. Noda, and T. Yoshimori. 2008a. An Atg4B mutant hampers the lipidation of LC3 paralogues and causes defects in autophagosome closure. *Mol. Biol. Cell.* 19:4651–4659. http://dx.doi.org/10.1091/mbc.E08-03-0312

Fujita, N., T. Itoh, H. Omori, M. Fukuda, T. Noda, and T. Yoshimori. 2008b. The Atg16L complex specifies the site of LC3 lipidation for membrane biogenesis in autophagy. *Mol. Biol. Cell.* 19:2092–2100. http://dx.doi.org/10.1091/mbc.E07-12-1257

Fujita, N., T. Saitoh, S. Kageyama, S. Akira, T. Noda, and T. Yoshimori. 2009. Differential involvement of Atg16L1 in Crohn disease and canonical autophagy: analysis of the organization of the Atg16L1 complex in fibroblasts. *J. Biol. Chem.* 284:32602–32609. http://dx.doi.org/10.1074/jbc.M109.037671

Fujita, N., and T. Yoshimori. 2011. Ubiquitination-mediated autophagy against invading bacteria. *Curr. Opin. Cell Biol.* 23:492–497. http://dx.doi.org/10.1016/j.ceb.2011.03.003

Hara, T., and N. Mizushima. 2009. Role of ULK-FIP200 complex in mammalian autophagy: FIP200, a counterpart of yeast Atg17? *Autophagy*. 5:85–87. http://dx.doi.org/10.4161/auto.5.1.7180

Hofmann, R.M., and C.M. Pickart. 1999. Noncanonical MMS2-encoded ubiquitin-conjugating enzyme functions in assembly of novel polyubiquitin chains for DNA repair. *Cell*. 96:645–653. http://dx.doi.org/10.1016/S0092-8674(00)80575-9

Huett, A., R.J. Heath, J. Begun, S.O. Sassi, L.A. Baxt, J.M. Vyas, M.B. Goldberg, and R.J. Xavier. 2012. The LRR and RING domain protein LRSAM1 is an E3 ligase crucial for ubiquitin-dependent autophagy of intracellular *Salmonella* Typhimurium. *Cell Host Microbe*. 12:778–790. http://dx.doi.org/10.1016/j.chom.2012.10.019

Itakura, E., and N. Mizushima. 2010. Characterization of autophagosome formation site by a hierarchical analysis of mammalian Atg proteins. *Autophagy*. 6:764–776. http://dx.doi.org/10.4161/auto.6.6.12709

Itakura, E., C. Kishi-Itakura, I. Koyama-Honda, and N. Mizushima. 2012. Structures containing Atg9A and the ULK1 complex independently target depolarized mitochondria at initial stages of Parkin-mediated mitophagy. *J. Cell Sci.* 125:1488–1499. http://dx.doi.org/10.1242/jcs.094110

Itoh, T., N. Fujita, E. Kanno, A. Yamamoto, T. Yoshimori, and M. Fukuda. 2008. Golgi-resident small GTPase Rab33B interacts with Atg16L and modulates autophagosome formation. *Mol. Biol. Cell.* 19:2916–2925. http://dx.doi.org/10.1091/mbc.E07-12-1231

Iwai, K., and F. Tokunaga. 2009. Linear polyubiquitination: a new regulator of NF-kappaB activation. *EMBO Rep.* 10:706–713. http://dx.doi.org/10.1038/embor.2009.144

Kageyama, S., H. Omori, T. Saitoh, T. Sone, J.L. Guan, S. Akira, F. Imamoto, T. Noda, and T. Yoshimori. 2011. The LC3 recruitment mechanism is separate from Atg9L1-dependent membrane formation in the autophagic response against *Salmonella*. *Mol. Biol. Cell.* 22:2290–2300. http://dx.doi.org/10.1091/mbc.E10-11-0893

Katzmann, D.J., M. Babst, and S.D. Emr. 2001. Ubiquitin-dependent sorting into the multivesicular body pathway requires the function of a conserved endosomal protein sorting complex, ESCRT-I. *Cell*. 106:145–155. http://dx.doi.org/10.1016/S0092-8674(01)00434-2

Kimura, S., N. Fujita, T. Noda, and T. Yoshimori. 2009. Monitoring autophagy in mammalian cultured cells through the dynamics of LC3. *Methods Enzymol.* 452:1–12. http://dx.doi.org/10.1016/S0076-6879(08)03601-X

Kobayashi, S., T. Kojidani, H. Osakada, A. Yamamoto, T. Yoshimori, Y. Hiraoka, and T. Haraguchi. 2010. Artificial induction of autophagy around polystyrene beads in nonphagocytic cells. *Autophagy*. 6:36–45. http://dx.doi.org/10.4161/auto.6.1.10324

Kuma, A., M. Hatano, M. Matsui, A. Yamamoto, H. Nakaya, T. Yoshimori, Y. Ohsumi, T. Tokuhisa, and N. Mizushima. 2004. The role of autophagy during the early neonatal starvation period. *Nature*. 432:1032–1036. http://dx.doi.org/10.1038/nature03029

Langelier, C., U.K. von Schwedler, R.D. Fisher, I. De Domenico, P.L. White, C.P. Hill, J. Kaplan, D. Ward, and W.I. Sundquist. 2006. Human ESCRT-II complex and its role in human immunodeficiency virus type 1 release. *J. Virol.* 80:9465–9480. http://dx.doi.org/10.1128/JVI.01049-06

Matsunaga, K., T. Saitoh, K. Tabata, H. Omori, T. Satoh, N. Kurotori, I. Maejima, K. Shirahama-Noda, T. Ichimura, T. Isobe, et al. 2009. Two Beclin 1-binding proteins, Atg14L and Rubicon, reciprocally regulate autophagy at different stages. *Nat. Cell Biol.* 11:385–396. http://dx.doi.org/10.1038/ncb1846

Mizushima, N. 2010. The role of the Atg1/ULK1 complex in autophagy regulation. *Curr. Opin. Cell Biol.* 22:132–139. http://dx.doi.org/10.1016/j.ceb.2009.12.004

Mizushima, N., A. Kuma, Y. Kobayashi, A. Yamamoto, M. Matsubae, T. Takao, T. Natsume, Y. Ohsumi, and T. Yoshimori. 2003. Mouse Apg16L, a novel WD-repeat protein, targets to the autophagic isolation membrane with the Apg12-Apg5 conjugate. *J. Cell Sci.* 116:1679–1688. http://dx.doi.org/10.1242/jcs.00381

Mizushima, N., B. Levine, A.M. Cuervo, and D.J. Klionsky. 2008. Autophagy fights disease through cellular self-digestion. *Nature*. 451:1069–1075. http://dx.doi.org/10.1038/nature06639

Morita, S., T. Kojima, and T. Kitamura. 2000. Plat-E: an efficient and stable system for transient packaging of retroviruses. *Gene Ther.* 7:1063–1066. http://dx.doi.org/10.1038/sj.gt.3301206

Newton, K., M.L. Matsumoto, I.E. Wertz, D.S. Kirkpatrick, J.R. Lill, J. Tan, D. Dugger, N. Gordon, S.S. Sidhu, F.A. Fellouse, et al. 2008. Ubiquitin chain editing revealed by polyubiquitin linkage-specific antibodies. *Cell*. 134:668–678. http://dx.doi.org/10.1016/j.cell.2008.07.039

Nishimura, T., T. Kaizuka, K. Cadwell, M.H. Sahani, T. Saitoh, S. Akira, H.W. Virgin, and N. Mizushima. 2013. FIP200 regulates targeting of Atg16L1 to the isolation membrane. *EMBO Rep.* 14:284–291. http://dx.doi.org/10.1038/embor.2013.6

Pashkova, N., L. Gakhar, S.C. Winistorfer, L. Yu, S. Ramaswamy, and R.C. Piper. 2010. WD40 repeat propellers define a ubiquitin-binding domain that regulates turnover of F box proteins. *Mol. Cell.* 40:433–443. http://dx.doi.org/10.1016/j.molcel.2010.10.018

Paz, I., M. Sachse, N. Dupont, J. Mounier, C. Cederfur, J. Enninga, H. Leffler, F. Poirier, M.C. Prevost, F. Lafont, and P. Sansonetti. 2010. Galectin-3, a marker for vacuole lysis by invasive pathogens. *Cell. Microbiol.* 12:530–544. http://dx.doi.org/10.1111/j.1462-5822.2009.01415.x

Saitoh, T., M. Nakayama, H. Nakano, H. Yagita, N. Yamamoto, and S. Yamaoka. 2003. TWEAK induces NF-kappaB2 p100 processing and long lasting NF-kappaB activation. *J. Biol. Chem.* 278:36005–36012. http://dx.doi.org/10.1074/jbc.M304266200

Saitoh, T., N. Fujita, M.H. Jang, S. Uematsu, B.G. Yang, T. Satoh, H. Omori, T. Noda, N. Yamamoto, M. Komatsu, et al. 2008. Loss of the autophagy protein Atg16L1 enhances endotoxin-induced IL-1beta production. *Nature*. 456:264–268. http://dx.doi.org/10.1038/nature07383

Saitoh, T., N. Fujita, T. Hayashi, K. Takahara, T. Satoh, H. Lee, K. Matsunaga, S. Kageyama, H. Omori, T. Noda, et al. 2009. Atg9a controls dsDNA-driven dynamic translocation of STING and the innate immune response. *Proc. Natl. Acad. Sci. USA*. 106:20842–20846. http://dx.doi.org/10.1073/pnas.0911267106

Shahnazari, S., W.L. Yen, C.L. Birmingham, J. Shiu, A. Namolovan, Y.T. Zheng, K. Nakayama, D.J. Klionsky, and J.H. Brumell. 2010. A diacylglycerol-dependent signaling pathway contributes to regulation of antibacterial autophagy. *Cell Host Microbe*. 8:137–146. http://dx.doi.org/10.1016/j.chom.2010.07.002

Suzuki, K., and Y. Ohsumi. 2010. Current knowledge of the pre-autophagosomal structure (PAS). *FEBS Lett.* 584:1280–1286. http://dx.doi.org/10.1016/j.febslet.2010.02.001

Thurston, T.L., G. Ryzhakov, S. Bloor, N. von Muhlinen, and F. Randow. 2009. The TBK1 adaptor and autophagy receptor NDP52 restricts the proliferation of ubiquitin-coated bacteria. *Nat. Immunol.* 10:1215–1221. http://dx.doi.org/10.1038/ni.1800

Thurston, T.L., M.P. Wandel, N. von Muhlinen, A. Foeglein, and F. Randow. 2012. Galectin 8 targets damaged vesicles for autophagy to defend cells against bacterial invasion. *Nature*. 482:414–418. http://dx.doi.org/10.1038/nature10744

Tokunaga, F., S. Sakata, Y. Saeki, Y. Satomi, T. Kirisako, K. Kamei, T. Nakagawa, M. Kato, S. Murata, S. Yamaoka, et al. 2009. Involvement of linear polyubiquitylation of NEMO in NF-kappaB activation. *Nat. Cell Biol.* 11:123–132. http://dx.doi.org/10.1038/ncb1821

van Wijk, S.J., E. Fiskin, M. Putyrski, F. Pampaloni, J. Hou, P. Wild, T. Kensche, H.E. Grecco, P. Bastiaens, and I. Dikic. 2012. Fluorescence-based sensors to monitor localization and functions of linear and K63-linked ubiquitin chains in cells. *Mol. Cell.* 47:797–809. http://dx.doi.org/10.1016/j.molcel.2012.06.017